

Analysis of Heterogeneous Wireless Networks Using Poisson Hard-Core Hole Process

Ian Flint, Han-Bae Kong, *Member, IEEE*, Nicolas Privault,
Ping Wang, *Senior Member, IEEE* and Dusit Niyato, *Fellow, IEEE*

Abstract

The Poisson point process (PPP) has been widely employed to model wireless networks and analyze their performance. The PPP has the property that nodes are conditionally independent from each other. As such, it may not be a suitable model for many networks where there exists a repulsion among the nodes. In order to address this limitation, we adopt a Poisson hard-core process (PHCP) in which no two nodes can be closer than a repulsion radius from one another. We consider two-tier heterogeneous networks where the spatial distributions of transmitters in the first-tier and the second-tier networks follow a PHCP and a PPP, respectively. To alleviate inter-tier interference, we consider a guard zone for the first-tier network and presume that the second-tier transmitters located in the zone are deactivated. Under this setup, the activated second-tier transmitters form a Poisson hard-core hole process. We first derive exact computable expressions of the coverage probability and introduce a method to efficiently evaluate the expressions. Then, we provide approximations of the coverage probability which have lower computational complexities. Additionally, as a special case, we investigate the coverage probability of single-tier networks by modeling the locations of transmitters as a PHCP.

Index Terms

Stochastic geometry, repulsive point process, Poisson hard-core process.

I. INTRODUCTION

Wireless communication networks have evolved to meet the requirement of high speed data services. As a promising network architecture capable of supporting the demand, heterogeneous

I. Flint and N. Privault are with the School of Physical and Mathematical Sciences, Nanyang Technological University, Singapore 639798 (e-mail: iflint@ntu.edu.sg; nprivault@ntu.edu.sg). H.-B. Kong, P. Wang and D. Niyato are with the School of Computer Science and Engineering, Nanyang Technological University, Singapore 639798 (e-mail: hbkong@ntu.edu.sg; wangping@ntu.edu.sg; dniyato@ntu.edu.sg). H.-B. Kong is the corresponding author. A part of this paper was presented at the *IEEE Int. Conf. on Commun. (ICC)*, Paris, France, May 2017 [1].

networks (HetNets) have attracted much attention [2]. Recently, many researchers have utilized stochastic geometry [3] to model and analyze wireless networks since conventional methods assuming a regular hexagonal lattice or the Wyner model [4] are unrealistic and difficult to apply.

A. Related Work and Motivations

The spatial distribution of nodes in wireless networks strongly affects the performance of networks. Since the assumption of independence among the nodes makes the performance analysis tractable, many works have attempted to analyze wireless networks by modeling the spatial distribution of the nodes as a Poisson point process (PPP) [5]–[12]. The authors in [5] and [6] characterized the transmission capacity of ad hoc wireless networks. In the case of cellular networks, downlink and uplink performances were studied in [7] and [8], respectively. However, in the PPP model, conditional on the PPP having n nodes, the nodes are assumed to be distributed independently from one another, making the PPP an unsuitable model when it comes to reflecting the actual node deployment in many wireless networks. In [7], it is shown that modeling the locations of cellular base stations (BSs) as a PPP underestimates the performance of the actual BS deployment.

In practical networks, the locations of transmitters may be chosen in order to alleviate interference or extend coverage region, and thus a repulsion among the locations of the transmitters naturally arises [13]–[16].¹ In this context, repulsive point processes which are either soft-core point processes [18]–[21] or hard-core point processes (HCPs) have drawn attention of researchers as models for actual networks which exhibit repulsion. The performance of cellular networks has been analyzed by modeling the locations of BSs as a determinantal point process (DPP) [18], a Ginibre point process (GPP) [19] and a β -GPP ($0 < \beta \leq 1$) [20]. The authors in [21] examined ambient radio frequency energy harvesting sensor networks using an α -GPP ($-1 \leq \alpha < 0$). Although the soft-core point processes can reflect repulsion, they cannot forbid points from being close to each others. Conversely, the HCPs are characterized by the property that no two points can be closer than a given repulsion radius to one another. Therefore, in this

¹For cellular networks, in order to serve hotspots area, the distribution of small cell BSs (SBSs) may exhibit a clustering nature [17]. In this paper, we focus on the case where there exists a repulsion rather than a clustering.

paper, we focus on the HCPs since its property is more suitable to model practical networks. We distinguish two main classes of HCPs which we now introduce.

The Matérn hard core process (MHCP) of type I [22] is obtained by retaining every point of a PPP which is not within the repulsion distance from another point of the PPP. The MHCP type II model [22] is constructed by assigning a uniform age $t \in [0, 1]$ to each point of a PPP and removing every point which is within the repulsion distance of a younger point of the PPP (a point x with age t_x is said to be younger than y with age t_y if $t_x \leq t_y$). In [23], it was shown that BS locations in wireless cellular networks are well modeled by MHCPs. The works in [24] and [25] studied mean interference of MHCPs of types I and II, respectively. The nearest neighbor distribution in the MHCP type II was derived in [26]. In addition, a modified MHCP has been applied to analyze carrier-sense multiple access with collision avoidance (CSMA/CA) networks [27]. Although the MHCP models the CSMA/CA networks well, exact expressions for key metrics are not available since the Laplace functional of the MHCP is unknown. As an example, it is intractable to find the exact distribution of the signal-to-noise-plus-interference ratio (SINR), which determines important performance metrics such as achievable rate and coverage probability, for the networks modeled by the MHCP as in [13], [28], [29].

A better suited HCP turns out to be the Poisson hard-core process (PHCP) [3] (sometimes called Gibbs hard-core process or Strauss hard-core process) which is a PPP conditional on all its points being further than a certain distance from one another. From the experimental results in [14]–[16], it was verified that the PHCP models the actual deployment of BSs which exhibits a repulsive behavior. However, previous works on the PHCP have only tried to fit the PHCP to real configurations of the nodes. We found that the performance of networks modeled by a PHCP has not been analytically investigated yet. Thus, in this paper, we introduce the exact expression of the coverage probability of the network modeled by the PHCP, and provide simple approximations of the coverage probability.

HetNets have emerged as an effective solution to meet high traffic demands and eliminate coverage dead zones. For downlink cellular HetNets, assuming that each tier is represented by a PPP, the coverage probability was identified in [9], and performance with flexible cell association was examined in [10]. Also, the works in [11] and [12] analyzed the success probability in downlink multiuser multiple-input multiple-output (MIMO) HetNets, and the outage probability of uplink multi-tier cellular networks, respectively. However, for analytical tractability, the works

in [9]–[12] assumed that the spatial distribution of BSs in a tier is independent from other tiers. In many practical networks, there exists a repulsion among the tiers since closely located BSs experience excessive interference, and therefore assuming the independence among the tiers may not be suitable for practical scenarios.

As a method to alleviate the interference, for wireless ad hoc networks, the concept of guard zone (also called exclusion zone), which is defined as the region around a receiver where transmissions are not allowed, was introduced in [30]. Let us consider two independent PPPs Φ_1 and Φ_2 . When the points in Φ_1 have disc-shaped exclusion zones, and only the points in Φ_2 outside the exclusion zones are activated, the activated points in Φ_2 form a Poisson hole process (PHP) [31]. By modeling the spatial distribution of cognitive transmitters as a PHP, the performance of cognitive radio networks was characterized in [31] and [32]. Also, the PHP was applied to a two-tier cellular network [33] and a D2D enhanced cellular network [34] to analyze the performance of the networks. Recently, the authors in [35] provided bounds for the Laplace transform of a PHP field of interferers. However, although the PHP takes the inter-tier interference into account, it fails to reflect a correlation among the points due to the PPP assumption. Furthermore, the works in [30]–[35] only derived the bounds of the performance rather than the exact expression. Therefore, in this paper, we consider a two-tier network with a PHCP and a guard zone, and introduce not only approximations but also an exact analytical representation of the performance.

B. Contributions and Organization

In this paper, we study two-tier HetNets. We assume that the locations of transmitters in the first-tier network are deployed to mitigate interference or extend the coverage region. Additionally, it is assumed that transmitters in the second-tier network are deployed in an unplanned fashion. Hence, we model the distributions of transmitters in the first- and second-tier networks as a PHCP and a PPP, respectively. Furthermore, a guard zone for the first-tier network, which deactivates the second-tier transmitters in the zone, is considered to alleviate the inter-tier interference. Under this setup, the activated second-tier transmitters form a *Poisson hard-core hole process* (PHCHP). The contributions of this paper are summarized next.

- First, we identify the Laplace transform of the interference at a typical user from the first-tier and the second-tier networks by exploiting the Laplace functional of pairwise interaction

point processes. Here, the interference field induced by the second-tier transmitters can be modeled as a PHCP. Then, in Theorem 1, we provide an exact computable expression of the coverage probability of two-tier HetNets which is the probability that SINR is larger than a certain target SINR threshold. The proof of Theorem 1 relies on a geometric argument which is detailed in Appendix D.

- Next, in Corollary 1, we specialize our result for the two-tier HetNets to the setting of single-tier networks consisting of transmitters following a PHCP by letting the intensity of the second-tier transmitters go to zero. We emphasize that even the performance of the single-tier networks with a PHCP has not been studied in the literature so far.
- We apply the Quasi-Monte Carlo (QMC) technique to compute the derived results. We confirm that our analytical results, which are evaluated by using the QMC technique, are well matched with the Monte Carlo simulation results.
- Lastly, we provide approximations of the coverage probability. We derive numerical approximations of the coverage probability which have a lower computational complexity and exhibit a negligible gap compared to the Monte Carlo simulation result. Then, we address probabilistic approximations by approximating an interference field by a composition of homogeneous PPPs with well chosen intensities, cf. Theorems 3 and 4.

The organization of this paper is as follows. In Section II, we introduce some background on pairwise interaction point processes and describe the system model. In Section III, we analyze the exact coverage probability of both single- and two-tier networks. Section IV provides our approximations of the coverage probability. In Section V, numerical simulation results are presented to validate our analytical results. Finally, the conclusions are given in Section VI.

The following notations are used throughout this paper. The operators $\|\cdot\|$ and \setminus indicate Euclidean 2-norm and set difference, respectively. The bold notation is used to denote a point $\mathbf{x} \in \mathbb{R}^2$. In addition, we denote by \mathbb{P} the probability on the underlying probability space, and the corresponding expectation is denoted by \mathbb{E} .

II. PRELIMINARIES AND SYSTEM MODEL

In this section, we first introduce fundamental properties of the pairwise interaction point process which includes the PHCP as a special case. Then, we present the system model by focusing on the PHCP.

A. Preliminaries

Let $W \subset \mathbb{R}^2$ be an observation window, and let Ψ be a point process on W , i.e., a random finite set of points located in W . Since many quantities manipulated in this manuscript depend only on the radii of the points in Ψ , a polar change of coordinates combined with a circular observation window allows us to present more compact closed forms. Therefore, in this paper, we assume that $W = \mathcal{B}_0(R)$ is a circular observation window of radius R centered at the origin $(0, 0)$ in \mathbb{R}^2 . The configuration space (i.e., all finite sets of points of W) is denoted by \mathcal{X} . We assume that Ψ has joint densities $f_\Psi : \mathcal{X} \rightarrow [0, \infty)$ [36], i.e.,

$$\mathbb{E}[F(\Psi)] = \sum_{n \geq 0} \frac{e^{-\pi R^2}}{n!} \int_{W^n} F(\{\mathbf{x}_1, \dots, \mathbf{x}_n\}) f_\Psi(\{\mathbf{x}_1, \dots, \mathbf{x}_n\}) d\mathbf{x}_1 \cdots d\mathbf{x}_n, \quad (1)$$

for all non-negative measurable functions $F : \mathcal{X} \rightarrow [0, \infty)$ where $d\mathbf{x}_i$ denotes the Lebesgue measure on W . We recall that the joint densities f_Ψ defined in (1) characterize the distribution of the point process.

In the following, we introduce the definitions of the pairwise interaction point process and the PHCP.

Definition 1 (Pairwise interaction point process [36]). *The point process Ψ is said to be a pairwise interaction point process if f_Ψ defined in (1) is given by*

$$f_\Psi(\omega) = c \prod_{\mathbf{x} \in \omega} \varphi_1(\mathbf{x}) \prod_{\{\mathbf{x}, \mathbf{y}\} \subset \omega} \varphi_2(\|\mathbf{x} - \mathbf{y}\|), \quad \omega \in \mathcal{X}. \quad (2)$$

Here, c is the normalizing constant defined by

$$c^{-1} \triangleq \sum_{n \geq 0} \frac{e^{-\pi R^2}}{n!} \int_{W^n} \prod_{i=1}^n \varphi_1(\mathbf{x}_i) \prod_{\substack{j, k=1, \dots, n; \\ j \neq k}} \varphi_2(\|\mathbf{x}_j - \mathbf{x}_k\|) d\mathbf{x}_1 \cdots d\mathbf{x}_n, \quad (3)$$

where φ_1 and φ_2 are two non-negative functions such that the right-hand side of (3) is finite. The function φ_1 plays the role of the (non-homogeneous) intensity while φ_2 is the physical interaction potential between the points of the point process.

Definition 2. *A pairwise interaction point process with $\varphi_1(\mathbf{x}) = \lambda$ and $\varphi_2(r) = \mathbb{1}_{\{r \geq d\}}$ is called a PHCP with intensity $\lambda > 0$ and radius $d > 0$. Here, $\mathbb{1}_A$ is the indicator function of the event A , i.e., the function equal to 1 if the event A holds, and 0 if not. The parameter λ is the intensity parameter, and the potential function φ_2 prohibits the PHCP from having any two points closer*

than d to one another. It can be shown that the probability of having a point in an infinitesimal volume $d\mathbf{x}$ at the location \mathbf{x} conditional on ω is $\lambda \mathbb{1}_{\{\mathbf{x} \notin \cup_{\mathbf{y} \in \omega} \mathcal{B}_{\mathbf{y}}(d)\}} d\mathbf{x}$, as the volume of $d\mathbf{x}$ goes to zero.

We define the intensity of the point process as the measurable function $\lambda : W \rightarrow [0, \infty)$ which satisfies $\mathbb{E}[\Psi(W)] = \int_W \lambda(\mathbf{x}) d\mathbf{x}$, i.e., the intensity of Ψ is the density of the (random) number of points. Note that by the Georgii-Nguyen-Zessin formula [37], we have

$$\lambda(\mathbf{x}) = \varphi_1(\mathbf{x}) \mathbb{E} \left[\prod_{\mathbf{y} \in \Psi} \varphi_2(\|\mathbf{x} - \mathbf{y}\|) \right], \quad \mathbf{x} \in W. \quad (4)$$

We further define the reduced Palm measure of Ψ at $\mathbf{x} \in W$ [36] by

$$\mu_{\mathbf{x}}(d\omega) \triangleq \varphi_1(\mathbf{x}) \prod_{\mathbf{y} \in \omega} \varphi_2(\|\mathbf{x} - \mathbf{y}\|) \lambda^{-1}(\mathbf{x}) \mathbb{P}_{\Psi}(d\omega), \quad \mathbf{x} \in W, \quad (5)$$

where \mathbb{P}_{Ψ} denotes the distribution of Ψ . To obtain some heuristics on the reduced Palm measure $\mu_{\mathbf{x}}$, let $d\mathbf{x}$ be a small volume around $\mathbf{x} \in W$, let A belong to the σ -algebra of sets of \mathcal{X} . Then, denoting by $|d\mathbf{x}|$ the volume of $d\mathbf{x}$, by the Georgii-Nguyen-Zessin formula, we have

$$\mu_{\mathbf{x}}(A) = \lim_{|d\mathbf{x}| \rightarrow 0} \mathbb{P}((\Psi \setminus d\mathbf{x}) \in A \mid |\Psi \cap d\mathbf{x}| = 1),$$

or to state things analogously, $\mu_{\mathbf{x}}$ is the distribution of the point process obtained by conditioning Ψ on $\mathbf{x} \in \Psi$ and removing \mathbf{x} from the resulting configuration. When Ψ is the PPP, $\mu_{\mathbf{x}} = \mathbb{P}_{\Psi}$, which is known in the literature as the Slivnyak-Mecke theorem [3]. We now characterize the reduced Palm measures of pairwise interaction point processes.

Proposition 1. *Let Ψ be a pairwise interaction point process with interaction functions φ_1 and φ_2 . Then, $\mu_{\mathbf{x}}$ is the law of a pairwise interaction point process with interaction functions given by*

$$\varphi_1^{\mathbf{x}}(\mathbf{y}) = \varphi_1(\mathbf{y}) \varphi_2(\|\mathbf{x} - \mathbf{y}\|) \text{ and } \varphi_2^{\mathbf{x}}(r) = \varphi_2(r). \quad (6)$$

Proof. For any measurable function $F : \mathcal{X} \rightarrow [0, \infty)$, by (5), we have

$$\int_{\mathcal{X}} F(\omega) \mu_{\mathbf{x}}(d\omega) = \varphi_1(\mathbf{x}) \lambda^{-1}(\mathbf{x}) \mathbb{E} \left[F(\Psi) \prod_{\mathbf{y} \in \Psi} \varphi_2(\|\mathbf{x} - \mathbf{y}\|) \right],$$

and by (1), we obtain

$$\begin{aligned} \int_{\mathcal{X}} F(\omega) \mu_{\mathbf{x}}(d\omega) &= c\varphi_1(\mathbf{x})\lambda^{-1}(\mathbf{x}) \sum_{n \geq 0} \frac{e^{-\pi R^2}}{n!} \int_{W^n} F(\{\mathbf{x}_1, \dots, \mathbf{x}_n\}) \\ &\quad \times \prod_{i=1}^n \varphi_1(\mathbf{x}_i) \varphi_2(\|\mathbf{x} - \mathbf{x}_i\|) \prod_{\substack{j,k=1,\dots,n; \\ j \neq k}} \varphi_2(\|\mathbf{x}_j - \mathbf{x}_k\|) d\mathbf{x}_1 \cdots d\mathbf{x}_n. \end{aligned} \quad (7)$$

Additionally, from (1) and (4), we have

$$\begin{aligned} \lambda(\mathbf{x}) &= \varphi_1(\mathbf{x}) \mathbb{E} \left[\prod_{\mathbf{y} \in \Psi} \varphi_2(\|\mathbf{x} - \mathbf{y}\|) \right] \\ &= c\varphi_1(\mathbf{x}) \sum_{n \geq 0} \frac{e^{-\pi R^2}}{n!} \int_{W^n} \prod_{i=1}^n \varphi_1(\mathbf{x}_i) \varphi_2(\|\mathbf{x} - \mathbf{x}_i\|) \prod_{\substack{j,k=1,\dots,n; \\ j \neq k}} \varphi_2(\|\mathbf{x}_j - \mathbf{x}_k\|) d\mathbf{x}_1 \cdots d\mathbf{x}_n. \end{aligned}$$

We conclude by comparing (7) to (1) and (2). \square

By Proposition 1 and Definition 2, the reduced Palm measure of the PHCP is the law of a pairwise interaction point process with interaction functions given by

$$\varphi_1^{\mathbf{x}}(\mathbf{y}) = \lambda \mathbb{1}_{\{\|\mathbf{x} - \mathbf{y}\| \geq d\}} \quad \text{and} \quad \varphi_2^{\mathbf{x}}(r) = \mathbb{1}_{\{r \geq d\}}. \quad (8)$$

We remark that the reduced Palm measure above corresponds to the distribution of a PPP with intensity λ on $W \setminus \mathcal{B}_{\mathbf{x}}(d)$ conditional on all its points lying farther than d from one-another.

We now discuss simulation methods producing points of a PHCP with intensity λ and radius d . In the naive simulation technique, the points are first generated according to a PPP with intensity λ , and then it is checked whether the minimum distance among the points is greater than d . If the minimum distance is less than d , the sample is rejected and another set of points is repeatedly generated until the minimum distance becomes larger than d . This contrasts with the simulation of an MHCP in which only one sample of the PPP is required. Since a potentially high number of samples of the PPP are rejected when λ , d or R are large, the naive simulation technique may not be efficient.

To overcome this issue, we adopt the perfect simulation algorithm in [38]. The algorithm starts from a PPP Z_0 with intensity λ , and constructs a backwards Markov chain $Z^j = \{Z_0^j, \dots, Z_j^j\}$, for $j = 0, -1, -2, \dots$. Then, two forward Markov chains are constructed, namely the upper process $U^j = \{U_j^j, \dots, U_0^j\}$ and the lower process $L^j = \{L_j^j, \dots, L_0^j\}$, respectively, where L_j^j is the null process and $U_j^j := Z_j^j$. The algorithm goes on until the two chains have converged

and yields a sample of the PHCP. The above perfect simulation algorithm is summarized in Algorithm 1.

Algorithm 1 Perfect simulation algorithm (simplified version of [38, p. 360])

- 1: Generate a PPP Z_0 on W with intensity λ and set $k = 1$;
 - 2: **repeat**
 - 3: Generate backwards $Z_{-2^{k-2}-1}, \dots, Z_{-2^{k-1}}$ according to [38, p. 356];
 - 4: Generate forwards $(L_{-2^{k-1}}, U_{-2^{k-1}}), \dots, (L_0^{-2^{k-1}}, U_0^{-2^{k-1}})$ according to (13)-(14) in [38];
 - 5: $k = k + 1$;
 - 6: **until** $U_0^{-2^{k-1}} = L_0^{-2^{k-1}}$
 - 7: **return** $U_0^{-2^{k-1}}$
-

Although the naive simulation technique may not be practical, it gives us an insight on the resulting intensity of the PHCP. Indeed, the naive algorithm has a tendency to reject configurations which have a high density of points, as these configurations will typically have points close to each others. Therefore, heuristically, the intensity of the resulting points of the PHCP (termed scaled intensity) ought to be less than λ . In the following lemma, we provide the scaled intensity for the reduced Palm measure of a PHCP and prove that it is indeed less than λ .

Lemma 1. *The scaled intensity of the reduced Palm measure of a PHCP with radius d and intensity λ is given by*

$$\tilde{\lambda}(\lambda, d) = \frac{\lambda}{\pi R^2} \frac{\sum_{n \geq 0} \frac{\lambda^n}{n!} \nu_{n+1}}{\sum_{n \geq 0} \frac{\lambda^n}{n!} \nu_n}, \quad (9)$$

where $\nu_n \triangleq \int_{(W \setminus \mathcal{B}_0(d))^n} \prod_{\substack{j,k=1,\dots,n; \\ j \neq k}} \mathbb{1}_{\{\|\mathbf{x}_j - \mathbf{x}_k\| \geq d\}} d\mathbf{x}_1 \cdots d\mathbf{x}_n$.

Proof. See Appendix A. □

By the inequality $\nu_{n+1} \leq \nu_n(\pi R^2 - \pi d^2) \leq \nu_n \pi R^2$, we obtain $\tilde{\lambda}(\lambda, d) \leq \lambda$, which formalizes the intuition that the scaled intensity $\tilde{\lambda}(\lambda, d)$ will be less than λ .

B. System model

We consider two-tier HetNets where the spatial distributions of transmitters in the first-tier and the second-tier networks follow a PHCP Ψ_1 and a PPP Ψ_2 on the observation window W ,

TABLE I
LIST OF SYMBOLS

| Symbol | Definition |
|-------------|--|
| Ψ_1 | PHCP which models the distribution of the transmitters in the first-tier network |
| Ψ_1^0 | Reduced Palm measure of Ψ_1 |
| Ψ_2 | PPP which models the distribution of the transmitters in the second-tier network |
| Ψ_2^a | Activated transmitters in the second-tier network |
| Ξ | Guard zone based on the locations of transmitters in Ψ_1^0 |
| λ_1 | Spatial intensity of PHCP Ψ_1 |
| λ_2 | Spatial intensity of PPP Ψ_2 |
| $d_{h.c.}$ | Radius of PHCP Ψ_1 |
| d_G | Radius of guard zone Ξ |
| r_1 | Distance between the typical receiver in the first-tier network and its associated transmitter |
| P_1 | Transmit power of the transmitters in the first-tier network |
| P_2 | Transmit power of the transmitters in the second-tier network |
| α | Path loss exponent |

respectively. A list of the symbols used in this paper is given in Table I. Ψ_1 is a PHCP with intensity λ_1 and radius $d_{h.c.}$ such that $0 \leq d_{h.c.} < R$, and Ψ_2 is a PPP with intensity λ_2 . with intensity λ_1 and radius $d_{h.c.}$ such that $0 \leq d_{h.c.} < R$.

Each transmitter $\mathbf{x} \in \Psi_1$ sends data to its corresponding receiver. We study the performance at a typical receiver \mathbf{x}_1 , and its associated transmitter in the first-tier network (termed tagged transmitter) is conditioned on being located at the origin. Correspondingly, we denote by Ψ_1^0 the point process of transmitters, conditioned on a transmitter being located at the origin. The distribution of Ψ_1^0 is the reduced Palm measure of Ψ_1 , i.e., a pairwise interaction point process characterized by (8). We assume that the typical receiver \mathbf{x}_1 is located at a distance r_1 from its transmitter, in a direction which is assumed to be uniformly distributed. In other words, the coordinates of \mathbf{x}_1 are given by $(r_1 \cos(U), r_1 \sin(U))$ where $U \sim \mathcal{U}([0, 2\pi])$ is a uniform random variable on $[0, 2\pi]$ independent from the other random variables. Note that the analytical results in this paper can be applied to networks in which the typical receiver is located at a random distance R_1 from the origin, and we have conditioned on $R_1 = r_1$.

We assume that the spatial distribution of transmitters in the second-tier network Ψ_2 is independent from Ψ_1^0 and is modeled by a PPP with intensity λ_2 since the locations of the transmitters in the second-tier network are assumed to be independent and uniformly distributed.

We consider the case in which the interferences at the receivers (associated to Ψ_1^0) caused by transmitters in Ψ_2 are not desirable. As a way to alleviate the interferences, we introduce a guard zone and assume that among Ψ_2 , the points located in the guard zone are deactivated.² One may construct the guard zone based on the locations of receivers in the first-tier network. However, in practical scenarios, it may be difficult for the transmitters in Ψ_2 to detect the locations of the receivers since the receivers may be passive [39].

In this context, we define the guard zone based on the locations of transmitters in Ψ_1^0 as

$$\Xi = \mathcal{B}_0(d_G) \cup \bigcup_{x \in \Psi_1^0} \mathcal{B}_x(d_G), \quad (10)$$

where $0 \leq d_G \leq d_{\text{h.c.}}/2$ is the guard zone radius. The union with $\mathcal{B}_0(d_G)$ appears since the first-tier transmitter at the origin also forms a guard zone for its receiver. The point process Ψ_2^a , which corresponds to the activated transmitters (which are not in the guard zone), is defined as

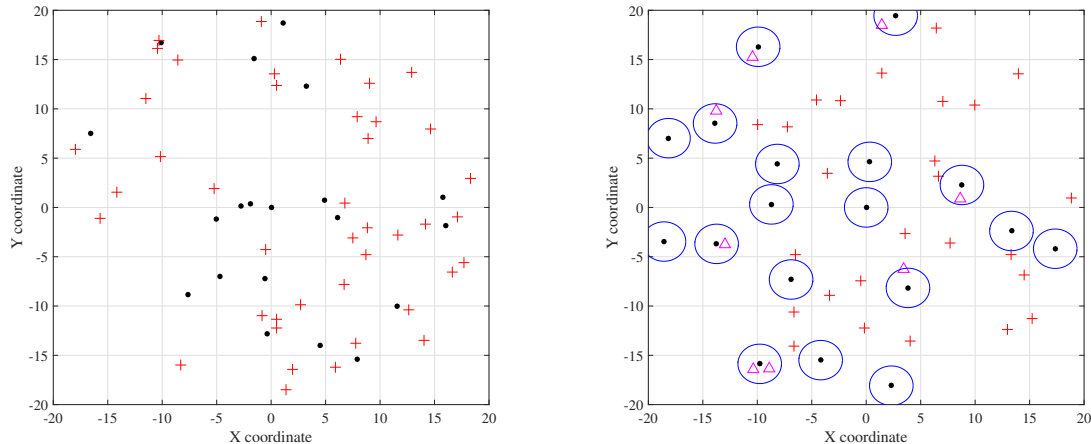
$$\Psi_2^a = \Psi_2 \setminus \Xi. \quad (11)$$

In this paper, we call Ψ_2^a a PHCHP. Compared to the PHP in [30]–[35], the PHCHP can take the repulsion among the transmitters in the first-tier network into account. Note that two transmitters in Ψ_1^0 cannot be at a distance less than $d_{\text{h.c.}}$ from one another, and an activated transmitter in Ψ_2^a cannot be closer than d_G to a point in Ψ_1^0 . However, there is no restriction on the distance between two transmitters in Ψ_2^a .

It is worth noting that our network model can be applied to cognitive networks where the distributions of primary and secondary transmitters are modeled as a PHCP and a PPP, respectively. As a way to ensure that the transmission from the secondary transmitters does not cause excessive interference to the primary transmission, one can construct exclusion zones around the primary transmitters which can be expressed as Ξ in (10). In this case, the activated secondary transmitters can be modeled as a PHCHP Ψ_2^a in (11).

In addition, we could consider two-tier closed-access cellular networks where macro cell BSs (MBSs) and SBSs follow a PHCP and a PPP, respectively, when a typical user is assumed to be

²A transmitter in Ψ_2 can know whether it is in the guard zone or not by checking the signal strength from the transmitters in the first-tier network.



(a) Two independent PPPs with intensities $\lambda_1 = 0.02$ and (b) A PHCP Ψ_1 with $\lambda_1 = 0.02$ and $d_{h.c.} = 4$, and Ψ_2 with $\lambda_2 = 0.04$ and $d_G = 2$.

Fig. 1. Some realizations of two-tier networks.

served by a MBS and its contact distance is equal to r_1^3 . When guard zones are created based on the locations of the MBSs, the spatial distribution of the activated SBSs follows a PHCHP Ψ_2^a in (11).

Fig. 1 illustrates realizations of the two-tier HetNets where dots and circles indicate the locations of the transmitters in the first-tier network and boundaries of the guard zone, respectively. The crosses and triangles denote the activated and deactivated transmitters in the second-tier network. As observed in Fig. 1, by employing the PHCP and guard zone, we can alleviate not only intra-tier interference but also inter-tier interference.

The quantities of interest are the interference from the other transmitters I and the SINR at the typical receiver γ , which can be written as

$$\gamma = \frac{P_1 h r_1^{-\alpha}}{I + \sigma^2}, \quad (12)$$

and

$$I = \sum_{\mathbf{y} \in \Psi_1^0} P_1 h_{\mathbf{y}} \|\mathbf{y} - \mathbf{x}_1\|^{-\alpha} + \sum_{\mathbf{z} \in \Psi_2^a} P_2 h_{\mathbf{z}} \|\mathbf{z} - \mathbf{x}_1\|^{-\alpha}, \quad (13)$$

³The generalization to an open-access cellular network with the identification of the distribution of the contact distance is an interesting future research topic. We expect that our work will be a good starting point for the future works on heterogeneous cellular networks based on a PHCP.

where P_1 , P_2 , α and σ^2 stand for the transmit power at the transmitters in Ψ_1^0 , the transmit power at transmitters in Ψ_2^a , the path-loss exponent and the power of additive white Gaussian noise (AWGN), respectively. Here, h and h_y indicate, respectively, the fading gains of the channel between the typical receiver and the tagged transmitter, and the channel between the receiver and the transmitter positioned at y . We assume that fading channels follow the Rayleigh distribution, and thus h and h_y are independent exponential random variables with unit mean.

We study the coverage probability \mathcal{P}_{cov} , defined as the probability that the SINR γ in (12) is larger than a certain threshold γ_{th} , i.e., $\mathcal{P}_{cov} \triangleq \mathbb{P}(\gamma \geq \gamma_{th})$. Since h is an exponential random variable with unit mean,

$$\mathcal{P}_{cov} = \mathbb{P}\left(h \geq \frac{\gamma_{th} r_1^\alpha}{P_1} (I + \sigma^2)\right) = \mathbb{E}\left[\exp\left(-\frac{\gamma_{th} r_1^\alpha}{P_1} (I + \sigma^2)\right)\right] = \exp\left(-\frac{\gamma_{th} r_1^\alpha \sigma^2}{P_1}\right) \mathcal{L}_I\left(\frac{\gamma_{th} r_1^\alpha}{P_1}\right), \quad (14)$$

where $\mathcal{L}_X(s) = \mathbb{E}[\exp(-sX)]$ stands for the Laplace transform of a random variable X .

We finally point out that the single-tier network setting can be obtained by letting the intensity of the second-tier network λ_2 go to zero. Then, the interference in (13) is simplified to $I = \sum_{y \in \Psi_1^0} P_1 h_y \|y - \mathbf{x}_1\|^{-\alpha}$.

Until now, we have introduced some background on the PHCP and presented the two-tier HetNets models. In the next section, we derive exact expressions of the coverage probability.

III. EXACT PERFORMANCE ANALYSIS

In this section, we investigate the coverage probability at the typical receiver which is connected to the transmitter at the origin. First, we state and prove the following theorem, which provides an exact computable expression of the coverage probability of the two-tier network.

Theorem 1. *In the two-tier network setting, the coverage probability \mathcal{P}_{cov} is given by*

$$\begin{aligned} \mathcal{P}_{cov} &= c \exp\left(-\frac{\gamma_{th} r_1^\alpha \sigma^2}{P_1} - \lambda_2 \kappa\right) \sum_{n \geq 0} \frac{\lambda_1^n}{n!} \int_{(W \setminus \mathcal{B}_0(d_{h.c.}))^n} \prod_{i=1}^n \frac{1}{1 + \gamma_{th} r_1^\alpha \|\mathbf{x}_i - (r_1, 0)\|^{-\alpha}} \\ &\times \prod_{\substack{j,k=1,\dots,n; \\ j \neq k}} \mathbb{1}_{\{\|\mathbf{x}_j - \mathbf{x}_k\| \geq d_{h.c.}\}} \exp\left(\lambda_2 \sum_{i=1}^n \int_0^{R+r_1} \frac{r \theta_{\mathbf{x}_i}(r)}{1 + P_1 (r/r_1)^\alpha / (\gamma_{th} P_2)} dr\right) d\mathbf{x}_1 \cdots d\mathbf{x}_n, \quad (15) \end{aligned}$$

where κ and $\theta_{\mathbf{x}_i}(r)$ have been defined in (37) and Proposition 3, respectively, and the normalizing constant c is equal to

$$c^{-1} \triangleq \sum_{n \geq 0} \frac{\lambda_1^n}{n!} \int_{(W \setminus \mathcal{B}_0(d_{h.c.}))^n} \prod_{\substack{j,k=1,\dots,n; \\ j \neq k}} \mathbb{1}_{\{\|\mathbf{x}_j - \mathbf{x}_k\| \geq d_{h.c.}\}} d\mathbf{x}_1 \cdots d\mathbf{x}_n. \quad (16)$$

Proof. See Appendix B. □

As a corollary, we derive the coverage probability (14) of single-tier networks.

Corollary 1. *In the single-tier network setting, the coverage probability \mathcal{P}_{cov} is given by*

$$\mathcal{P}_{cov} = c \exp\left(-\frac{\gamma_{th} r_1^\alpha \sigma^2}{P_1}\right) \sum_{n \geq 0} \frac{\lambda_1^n}{n!} \int_{(W \setminus \mathcal{B}_0(d_{h.c.}))^n} \prod_{\substack{j,k=1,\dots,n; \\ j \neq k}} \mathbb{1}_{\{\|\mathbf{x}_j - \mathbf{x}_k\| \geq d_{h.c.}\}} \quad (17)$$

$$\times \prod_{i=1}^n \frac{1}{1 + \gamma_{th} r_1^\alpha \|\mathbf{x}_i - (r_1, 0)\|^{-\alpha}} d\mathbf{x}_1 \cdots d\mathbf{x}_n,$$

where the normalizing constant c has been defined in (16).

Proof. We can prove the result by letting λ_2 in (15) go to zero in the two-tier setting. □

We now comment on the general result obtained in Theorem 1. First, we remark that the series in (15) is in fact a finite sum. To see this, note that for n large enough, the term $\prod_{\substack{j,k=1,\dots,n; \\ j \neq k}} \mathbb{1}_{\{\|\mathbf{x}_j - \mathbf{x}_k\| \geq d_{h.c.}\}}$ is equal to zero for all $\mathbf{x}_1, \dots, \mathbf{x}_n$. A similar comment can be made regarding the series in (16).

Next, we emphasize that the expressions in (15)-(17) contain multi-dimensional integrals, which may incur a high computational complexity, especially since the integrals are nested. We employ the QMC integration technique [40] to approximate the multi-dimensional integrals efficiently. For all $g : [0, 1]^n \rightarrow \mathbb{C}$, the QMC integration method exhibits a deterministic sequence $\mathbf{x}_1, \dots, \mathbf{x}_{N_s} \in [0, 1]^n$ such that

$$\frac{1}{N_s} \sum_{n=1}^{N_s} g(\mathbf{x}_n) \approx \int_{[0,1]^n} g(\mathbf{z}) d\mathbf{z}, \quad (18)$$

when N_s goes to infinity. The advantage of this method compared to the Monte-Carlo method (in which the sequence \mathbf{x}_n is stochastic) is that, for high dimensions, the QMC approximation converges much faster. In this paper, we choose the Sobol sequence [41] as the deterministic sequence. Since the QMC method is applicable for integrations over the unit square, we rewrite the expressions in Theorem 1 in the following corollary. Utilizing the results in Corollary 2 and the QMC integration method in (18), we can readily evaluate the coverage probability.

Corollary 2. *By changing the integral region in (15), we have*

$$\begin{aligned}
\mathcal{P}_{cov} &= c \exp\left(-\frac{\gamma_{th} r_1^\alpha \sigma^2}{P_1} - \lambda_2 \kappa\right) \sum_{n \geq 0} \frac{\lambda_1^n}{n!} (2R)^{2n} \int_{([0,1] \times [0,1])^n} \prod_{i=1}^n \mathbb{1}_{\{d_{h.c.}/(2R) \leq \|\mathbf{z}_i - (1/2, 1/2)\| \leq 1/2\}} \\
&\quad \times \prod_{i=1}^n \frac{1}{1 + s P_1 \|R(2\mathbf{z}_i - (1, 1)) - (r_1, 0)\|^{-\alpha}} \prod_{\substack{j,k=1,\dots,n; \\ j \neq k}} \mathbb{1}_{\{\|\mathbf{z}_j - \mathbf{z}_k\| \geq d_{h.c.}/(2R)\}} \\
&\quad \times \exp\left(\lambda_2 \sum_{i=1}^n \int_0^{R+r_1} \frac{r \theta_{R(2\mathbf{z}_i - (1,1))}(r)}{1 + P_1 (r/r_1)^\alpha / (\gamma_{th} P_2)} dr\right) d\mathbf{z}_1 \cdots d\mathbf{z}_n, \tag{19}
\end{aligned}$$

where

$$\begin{aligned}
c^{-1} &= \sum_{n \geq 0} \frac{\lambda_1^n (2R)^{2n}}{n!} \int_{([0,1] \times [0,1])^n} \prod_{i=1}^n \mathbb{1}_{\{d_{h.c.}/(2R) \leq \|\mathbf{z}_i - (1/2, 1/2)\| \leq 1/2\}} \\
&\quad \times \prod_{\substack{j,k=1,\dots,n; \\ j \neq k}} \mathbb{1}_{\{\|\mathbf{z}_j - \mathbf{z}_k\| \geq d_{h.c.}/(2R)\}} d\mathbf{z}_1 \cdots d\mathbf{z}_n. \tag{20}
\end{aligned}$$

Proof. The proof is obtained by doing a change of variables in (15) and (16). The details are omitted since the derivation is straightforward. \square

Letting λ_2 go to zero in Corollary 2, one can rewrite (17) so that the integrations are on powers of the unit square, thereby enabling us to apply the QMC method, cf. Fig 2 in Section V. The details are omitted for brevity.

IV. APPROXIMATIONS OF THE COVERAGE PROBABILITY

As observed in Section III, the exact expressions of the coverage probability may induce heavy complexity burdens. To this end, in this section, we provide approximations of the coverage probability which have lower computational complexity.

A. Numerical approximations

In this subsection, we provide numerical approximations of the coverage probability in (15) and (17). Our numerical approximation is based on two different insights. First, for any two sets $A, B \subset \mathbb{R}^d$ and any non-negative measurable function $f : \mathbb{R}^d \rightarrow [0, \infty)$, we use

$$\int_{A \cap B} f(\mathbf{z}) d\mathbf{z} \simeq \int_{A \cap B} \frac{1}{|A|} \int_A f(\mathbf{y}) d\mathbf{y} d\mathbf{z} = \frac{|A \cap B|}{|A|} \int_A f(\mathbf{y}) d\mathbf{y}, \tag{21}$$

where $|A|$ denotes the volume of the set A . The approximation (21) consists in approximating $f(\mathbf{z})$ by its average value on A . It is a good approximation when f does not vary much on $A \cap B$ or when $|A \cap B| \simeq |A|$. Second, by induction, we obtain the following approximation:

$$\begin{aligned}
& \int_{(W \setminus \mathcal{B}_0(d_{\text{h.c.}}))^n} \prod_{\substack{j,k=1,\dots,n; \\ j \neq k}} \mathbb{1}_{\{\|\mathbf{x}_j - \mathbf{x}_k\| \geq d_{\text{h.c.}}\}} d\mathbf{x}_1 \cdots d\mathbf{x}_n \\
&= \int_{(W \setminus \mathcal{B}_0(d_{\text{h.c.}}))^{n-1}} \prod_{\substack{j,k=2,\dots,n; \\ j \neq k}} \mathbb{1}_{\{\|\mathbf{x}_j - \mathbf{x}_k\| \geq d_{\text{h.c.}}\}} \left(\int_{W \setminus \mathcal{B}_0(d_{\text{h.c.}})} \mathbb{1}_{\{\mathbf{x}_1 \notin \bigcap_{i=2}^n \mathcal{B}_{\mathbf{x}_i}(d_{\text{h.c.}})\}} d\mathbf{x}_1 \right) d\mathbf{x}_2 \cdots d\mathbf{x}_n \\
&= \int_{(W \setminus \mathcal{B}_0(d_{\text{h.c.}}))^{n-1}} \prod_{\substack{j,k=2,\dots,n; \\ j \neq k}} \mathbb{1}_{\{\|\mathbf{x}_j - \mathbf{x}_k\| \geq d_{\text{h.c.}}\}} \left| W \setminus \mathcal{B}_0(d_{\text{h.c.}}) \setminus \left(\bigcap_{i=2}^n \mathcal{B}_{\mathbf{x}_i}(d_{\text{h.c.}}) \right) \right| d\mathbf{x}_2 \cdots d\mathbf{x}_n \\
&\simeq \max\left(0, (\pi R^2 - n\pi d_{\text{h.c.}}^2)\right) \int_{(W \setminus \mathcal{B}_0(d_{\text{h.c.}}))^{n-1}} \prod_{\substack{j,k=2,\dots,n; \\ j \neq k}} \mathbb{1}_{\{\|\mathbf{x}_j - \mathbf{x}_k\| \geq d_{\text{h.c.}}\}} d\mathbf{x}_2 \cdots d\mathbf{x}_n \\
&\simeq \prod_{k=1}^n (\pi R^2 - k\pi d_{\text{h.c.}}^2) \mathbb{1}_{\{n \leq R^2/d_{\text{h.c.}}^2\}}. \tag{22}
\end{aligned}$$

Utilizing (21) and (22), we obtain the following approximation.

Theorem 2. *In the two-tier network setting, the coverage probability is approximated by*

$$\begin{aligned}
\mathcal{P}_{\text{cov}} &\simeq c \exp\left(-\frac{\gamma_{\text{th}} r_1^\alpha \sigma^2}{P_1} - \lambda_2 \kappa\right) \sum_{n=0}^{\lfloor R^2/d_{\text{h.c.}}^2 \rfloor} \frac{\lambda_1^n \prod_{k=1}^n (R^2 - kd_{\text{h.c.}}^2)}{n! (R^2 - d_{\text{h.c.}}^2)^n} \\
&\quad \times \left(\int_{W \setminus \mathcal{B}_0(d_{\text{h.c.}})} \frac{1}{1 + \gamma_{\text{th}} r_1^\alpha \|\mathbf{x} - (r_1, 0)\|^{-\alpha}} \exp\left(\lambda_2 \int_0^{R+r_1} \frac{r \theta_{\mathbf{x}}(r)}{1 + P_1 (r/r_1)^\alpha / (\gamma_{\text{th}} P_2)} dr\right) d\mathbf{x} \right)^n \tag{23}
\end{aligned}$$

where $\lfloor a \rfloor$ denotes the largest integer smaller than $a \in \mathbb{R}$. Here, κ and $\theta_{\mathbf{x}_i}(r)$ have been defined in (37) and Proposition 3, respectively. The inverse of the normalizing constant is additionally approximated by

$$c^{-1} \simeq \sum_{n=0}^{\lfloor R^2/d_{\text{h.c.}}^2 \rfloor} \frac{(\pi \lambda_1)^n}{n!} \prod_{k=1}^n (R^2 - kd_{\text{h.c.}}^2). \tag{24}$$

Proof. Focusing on the approximation of multi-dimensional integral in (15), we set

$$A = (W \setminus \mathcal{B}_0(d_{\text{h.c.}}))^n, \quad B = \{(\mathbf{x}_1, \dots, \mathbf{x}_n) \in \mathbb{R}^{2n} : \forall i, j \in \{1, \dots, n\}, i \neq j, \|\mathbf{x}_i - \mathbf{x}_j\| \geq d_{\text{h.c.}}\},$$

and

$$f(\mathbf{x}_1, \dots, \mathbf{x}_n) = \prod_{i=1}^n \frac{1}{1 + \gamma_{\text{th}} r_1^\alpha \|\mathbf{x}_i - (r_1, 0)\|^{-\alpha}} \exp\left(\lambda_2 \sum_{i=1}^n \int_0^{R+r_1} \frac{r \theta_{\mathbf{x}_i}(r)}{1 + P_1 (r/r_1)^\alpha / (\gamma_{\text{th}} P_2)} dr\right).$$

By (21) and (22), we have

$$\begin{aligned}
\int_{A \cap B} f(\mathbf{z}) \, d\mathbf{z} &\simeq \frac{|A \cap B|}{|A|} \int_A f(\mathbf{y}) \, d\mathbf{y} \\
&= \frac{\int_{(W \setminus \mathcal{B}_0(d_{\text{h.c.}}))^n \prod_{\substack{j,k=1,\dots,n; \\ j \neq k}} \mathbb{1}_{\{\|\mathbf{x}_j - \mathbf{x}_k\| \geq d_{\text{h.c.}}\}} \, d\mathbf{x}_1 \cdots d\mathbf{x}_n}{(\pi R^2 - \pi d_{\text{h.c.}}^2)^n} \int_A f(\mathbf{y}) \, d\mathbf{y} \\
&\simeq \mathbb{1}_{\{n \leq R^2/d_{\text{h.c.}}^2\}} \frac{\prod_{k=1}^n (\pi R^2 - k\pi d_{\text{h.c.}}^2)}{(\pi R^2 - \pi d_{\text{h.c.}}^2)^n} \int_A f(\mathbf{y}) \, d\mathbf{y} \\
&= \mathbb{1}_{\{n \leq R^2/d_{\text{h.c.}}^2\}} \frac{\prod_{k=1}^n (R^2 - kd_{\text{h.c.}}^2)}{(R^2 - d_{\text{h.c.}}^2)^n} \int_A f(\mathbf{y}) \, d\mathbf{y}.
\end{aligned}$$

The above approximation yields (23). The approximation of the inverse of the normalizing constant follows from a direct application of (22). \square

We specialize the approximation in Theorem 2 to the single-tier network setting in the following corollary.

Corollary 3. *In single-tier networks, the coverage probability is approximated by*

$$\begin{aligned}
\mathcal{P}_{\text{cov}} &\simeq c \exp\left(-\frac{\gamma_{\text{th}} r_1^\alpha \sigma^2}{P_1}\right) \sum_{n=0}^{\lfloor R^2/d_{\text{h.c.}}^2 \rfloor} \frac{\lambda_1^n \prod_{k=1}^n (R^2 - kd_{\text{h.c.}}^2)}{n! (R^2 - d_{\text{h.c.}}^2)^n} \left(2\pi \int_{\max(d_{\text{h.c.}}, -r_1, 0)}^{R-r_1} \frac{r}{1 + \gamma_{\text{th}}(r_1/r)^\alpha} \, dr \right. \\
&\quad \left. + 2 \int_{R-r_1}^{r_1+R} \frac{\arccos\left(\frac{r_1^2+r^2-R^2}{2r_1r}\right)}{1 + \gamma_{\text{th}}(r_1/r)^\alpha} r \, dr - 2 \int_{|d_{\text{h.c.}}-r_1|}^{r_1+d_{\text{h.c.}}} \frac{\arccos\left(\frac{r_1^2+r^2-d_{\text{h.c.}}^2}{2r_1r}\right)}{1 + \gamma_{\text{th}}(r_1/r)^\alpha} r \, dr \right)^n, \quad (25)
\end{aligned}$$

where the normalizing constant c is approximated by (24).

Proof. By letting λ_2 go to zero in Theorem 2, we obtain

$$\begin{aligned}
\mathcal{P}_{\text{cov}} &\simeq c \exp\left(-\frac{\gamma_{\text{th}} r_1^\alpha \sigma^2}{P_1}\right) \\
&\quad \times \sum_{n=0}^{\lfloor R^2/d_{\text{h.c.}}^2 \rfloor} \frac{\lambda_1^n \prod_{k=1}^n (R^2 - kd_{\text{h.c.}}^2)}{n! (R^2 - d_{\text{h.c.}}^2)^n} \left(\int_{W \setminus \mathcal{B}_0(d_{\text{h.c.}})} \frac{1}{1 + \gamma_{\text{th}} r_1^\alpha \|\mathbf{x} - (r_1, 0)\|^{-\alpha}} \, d\mathbf{x} \right)^n.
\end{aligned}$$

Then, we derive the expression in (25) by applying Proposition 3 of Appendix D. \square

Note that the above approximations have low computational complexities compared to the results in Section III. More specifically, the approximation in Theorem 2 is a finite sum of terms involving a single three-dimensional integral. In single-tier networks, the approximation in Corollary 3 requires only the computation of a one-dimensional integral. In Section V, it will be shown numerically that the approximations in (23) and (25) are very tight.

B. Probabilistic approximation

In this subsection, we provide probabilistic approximations of the coverage probability which give us some insight on the coverage probability. The main difficulty in identifying the closed-form expression of the coverage probability $\mathcal{P}_{cov} = \exp\left(-\frac{\gamma_{th} r_1^\alpha \sigma^2}{P_1}\right) \mathcal{L}_I\left(\frac{\gamma_{th} r_1^\alpha}{P_1}\right)$ in (14) comes from the fact that the Laplace transform of the interference contains a sum of multi-dimensional integrals. Therefore, our idea is to approximate Ψ_1^0 and Ψ_2^a by PPPs in order to obtain simple expressions of the Laplace transform of the interference. In the following proposition we introduce a simple expression for a quantity related to \mathcal{L}_I which will be used in the following.

Proposition 2. *Let us assume that Φ is a PPP on W with intensity λ . Then, for $\tau \geq 0$ and $s > 0$, we have*

$$\mathbb{E} \left[\exp \left(-s \sum_{\mathbf{y} \in \Phi} h_{\mathbf{y}} \|\mathbf{y} - \mathbf{x}_1\|^{-\alpha} \mathbb{1}_{\{\|\mathbf{y} - \mathbf{x}_1\| \geq \tau\}} \right) \right] = f(\lambda, s, \tau),$$

where

$$f(\lambda, s, \tau) \triangleq \exp \left(-2\pi\lambda \int_{\tau}^{R-r_1} \frac{r}{1+s^{-1}r^\alpha} dr - 2\lambda \int_{R-r_1}^{r_1+R} \frac{\arccos\left(\frac{r_1^2+r^2-R^2}{2r_1r}\right)}{1+s^{-1}r^\alpha} r dr \right), \quad (26)$$

where $\arccos(x) \triangleq \cos^{-1}(x)$ is the inverse cosine function.

Proof. See Appendix C. □

We first concentrate on single-tier networks, and then consider two-tier networks. As one of the most naive approaches, one may substitute the locations of the points in Ψ_1^0 by a PPP on W denoted by $\Phi^{(1)}$ with intensity λ_1 . In this case, by Proposition 2, the Laplace transform of the interference can be approximated by $f(\lambda_1, sP_1, 0)$.

A more elaborate approach follows an idea from [42] which we recall. Since the transmitters in Ψ_1^0 cannot be at a distance less than $d_{h.c.}$ from one another, and the distance from a transmitter in Ψ_1^0 to its corresponding receiver is equal to r_1 , the distance between a receiver and its interfering transmitter is always larger than $\tau = \max(d_{h.c.} - r_1, 0)$. We could thus approximate Ψ_1^0 by the PPP $\Phi^{(1)}$ in which we remove the points which are closer than τ from \mathbf{x}_1 . By Proposition 2, the corresponding Laplace transform of the interference is

$$\mathbb{E} \left[\exp \left(-s \sum_{\mathbf{y} \in \Phi^{(1)}} P_1 h_{\mathbf{y}} \|\mathbf{y} - \mathbf{x}_1\|^{-\alpha} \mathbb{1}_{\{\|\mathbf{y} - \mathbf{x}_1\| \geq \tau\}} \right) \right] = f(\lambda_1, sP_1, \tau). \quad (27)$$

The last enhancement that we propose is to approximate Ψ_1^0 by a PPP $\Phi^{(2)}$ with intensity $\tilde{\lambda}(\lambda_1, d_{\text{h.c.}})$, the intensity of the reduced Palm measure of a PHCP, cf. Lemma 1. Summarizing the above discussion, we obtain the following probabilistic approximation.

Theorem 3. *In single-tier networks, the coverage probability is approximated by*

$$\begin{aligned} \mathcal{P}_{\text{cov}} &\simeq \exp\left(-\frac{\gamma_{\text{th}} r_1^\alpha \sigma^2}{P_1}\right) \mathbb{E} \left[\exp \left(-\gamma_{\text{th}} r_1^\alpha \sum_{\mathbf{y} \in \Phi^{(2)}} h_{\mathbf{y}} \|\mathbf{y} - \mathbf{x}_1\|^{-\alpha} \mathbb{1}_{\{\|\mathbf{y} - \mathbf{x}_1\| \geq \tau\}} \right) \right] \\ &= \exp\left(-\frac{\gamma_{\text{th}} r_1^\alpha \sigma^2}{P_1}\right) f(\tilde{\lambda}(\lambda_1, d_{\text{h.c.}}), \gamma_{\text{th}} r_1^\alpha, \tau), \end{aligned} \quad (28)$$

where $\tilde{\lambda}(\lambda_1, d_{\text{h.c.}})$ has been defined in Lemma 1 and $\tau = \max(d_{\text{h.c.}} - r_1, 0)$.

Now, we present the probabilistic approximation of the two-tier network. First of all, we assume that the interferences from Ψ_1^0 and Ψ_2^a are independent. Under this assumption, \mathcal{P}_{cov} becomes

$$\mathcal{P}_{\text{cov}} \simeq \exp\left(-\frac{\gamma_{\text{th}} r_1^\alpha \sigma^2}{P_1}\right) \mathcal{L}_{I_1} \left(\frac{\gamma_{\text{th}} r_1^\alpha}{P_1} \right) \mathcal{L}_{I_2} \left(\frac{\gamma_{\text{th}} r_1^\alpha}{P_1} \right), \quad (29)$$

where $I_1 = \sum_{\mathbf{y} \in \Psi_1^0} P_1 h_{\mathbf{y}} \|\mathbf{y} - \mathbf{x}_1\|^{-\alpha}$ and $I_2 = \sum_{\mathbf{z} \in \Psi_2^a} P_2 h_{\mathbf{z}} \|\mathbf{z} - \mathbf{x}_1\|^{-\alpha}$. Here, as described in the single-tier setting, $\mathcal{L}_{I_1}(s)$ can be approximated by $f(\tilde{\lambda}(\lambda_1, d_{\text{h.c.}}), sP_1, \tau)$. Now, we approximate Ψ_2^a by a PPP in order to find a simple approximation of \mathcal{L}_{I_2} .

The naive approach is to approximate Ψ_2^a by a PPP with intensity λ_2 , from which we deduce an approximation of $\mathcal{L}_{I_2}(s)$ given by $f(\lambda_2, sP_2, 0)$. Note that this approach overestimates the intensity of the interfering transmitters in the second-tier network. Since a portion of the transmitters in Ψ_2 becomes inactive due to the guard zone Ξ in (10), the intensity of the interfering second-tier transmitters $\tilde{\lambda}_2$ should be less than λ_2 , i.e., $\tilde{\lambda}_2 < \lambda_2$. In this context, we provide a better choice of intensity. First, note that the guard zone introduced in (10) has $\Psi_1^0(W) + 1$ points, and thus

$$\mathbb{E}[\Psi_1^0(W) + 1] = \tilde{\lambda}(\lambda_1, d_{\text{h.c.}}) \ell(W) + 1 = (\tilde{\lambda}(\lambda_1, d_{\text{h.c.}}) + (\pi R^2)^{-1}) \pi R^2,$$

which implies that the intensity of the guard zone is given by

$$\hat{\lambda}_1 \triangleq \tilde{\lambda}(\lambda_1, d_{\text{h.c.}}) + (\pi R^2)^{-1}. \quad (30)$$

Second, we remark that $\{\mathcal{B}_{\mathbf{x}}(d_G)\}_{\mathbf{x} \in \Psi_1^0 \cup (0,0)}$ are not overlapping, and thus the transmitters in Ψ_2 will be activated with a probability $1 - \pi d_G^2 \hat{\lambda}_1$. Hence, it is reasonable to approximate Ψ_2^a by a

PPP with intensity

$$\hat{\lambda}_2 = \lambda_2 \left(1 - \pi d_G^2 \tilde{\lambda}_1 - \left(\frac{d_G}{R} \right)^2 \right). \quad (31)$$

The corresponding approximation of $\mathcal{L}_{I_2}(s)$ is $f(\hat{\lambda}_2, sP_2, 0)$.

Lastly, since the distance between the typical receiver and a point in Ψ_2^a is always larger than $\hat{\tau} = \max(d_G - r_1, 0)$, similarly to (27), we obtain the following approximation.

Theorem 4. *In two-tier networks, the coverage probability is approximated by*

$$\mathcal{P}_{cov} \simeq \exp\left(-\frac{\gamma_{th} r_1^\alpha \sigma^2}{P_1}\right) f(\tilde{\lambda}(\lambda_1, d_{h.c.}), \gamma_{th} r_1^\alpha, \tau) f(\hat{\lambda}_2, \gamma_{th} r_1^\alpha P_2/P_1, \hat{\tau}), \quad (32)$$

where $\tilde{\lambda}(\lambda_1, d_{h.c.})$ has been defined in Lemma 1, $\hat{\lambda}_2$ is given by (31), $\tau = \max(d_{h.c.} - r_1, 0)$ and $\hat{\tau} = \max(d_G - r_1, 0)$.

Due to the simple expression in (28), we can see that the approximation in (28) is a decreasing function of λ_1 as $f(\lambda, s, \tau)$ in (26) is decreasing in λ . Likewise, the approximation in (32) becomes smaller with the increase in λ_2 since $\hat{\lambda}_2$ in (31) is proportional to λ_2 . Also, the approximation in (32) is a non-decreasing function of d_G since a larger d_G results in an increase in $\hat{\tau}$ and a decrease in $\hat{\lambda}_2$.

Let us conclude this section by addressing the complexity issue in detail. First, the conventional Monte Carlo integration with the results in Theorem 1 and Corollary 1 converges at a rate $O(1/\sqrt{n})$. Next, the convergence rate of the QMC method applied to Corollary 2 is in $O(\ln^k(n)/n)$ for a constant k [43], and therefore we can calculate the coverage probability more rapidly using the QMC method. Since the approximation in Theorem 2 contains a three-dimensional integral of a smooth function, it converges at a rate which is exponential in the number of quadrature points. Lastly, for the same reason, the convergence rates of the approximations in Corollary 3 and Section IV-B are also exponential in the number of quadrature points.

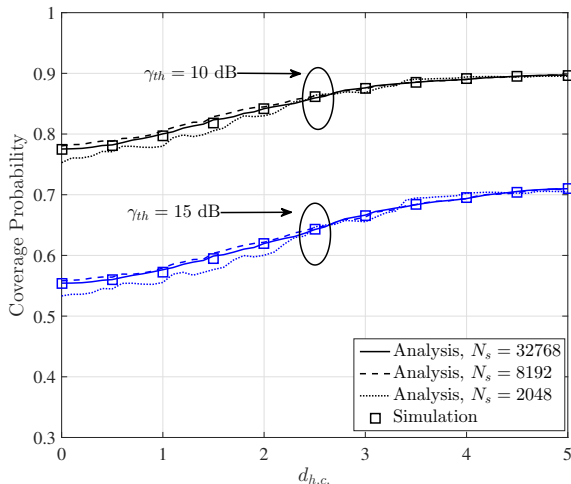


Fig. 2. Coverage probability of single-tier networks with different values of N_s .

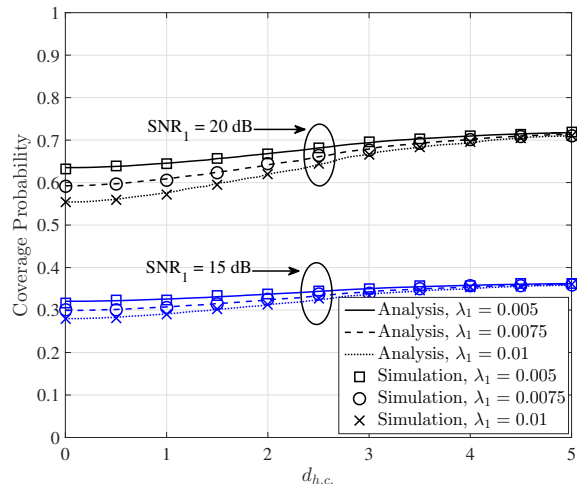


Fig. 3. Coverage probability of single-tier networks as a function of $d_{h.c.}$.

V. SIMULATION RESULTS

In this section, we provide numerical results to validate our analysis. Let us define $\text{SNR}_1 = P_1/\sigma^2$ and $\text{SNR}_2 = P_2/\sigma^2$. We set $\alpha = 4$, $r_1 = 1$, $\sigma^2 = 1$ and $R = 20^4$. The analytical results in (15) and (17) are evaluated by using the QMC method in (18) and the result in (19). Note that the performance of networks with $d_{h.c.} = 0$ can be interpreted as that of networks with a PPP.

In Figs. 2 to 5, we present the coverage probability of single-tier networks. Fig. 2 examines the coverage probability \mathcal{P}_{cov} with various numbers of terms in the Sobol sequence N_s when $\text{SNR}_1 = 20$ dB and $\lambda_1 = 0.01$. It is shown that the analytical results with $N_s = 2^{15}$ (32768) are well matched with the simulated results. Accordingly, in this paper, we set the number of terms in the Sobol sequences N_s as $N_s = 2^{15}$. From Fig. 2, we can see that \mathcal{P}_{cov} becomes larger as γ_{th} decreases and $d_{h.c.}$ grows. Also, it is shown that the impact of $d_{h.c.}$ is more pronounced when γ_{th} is high.

In Fig. 3, we plot the coverage probability \mathcal{P}_{cov} for different values of SNR_1 and λ_1 in the case of $\gamma_{th} = 15$ dB. We observe that \mathcal{P}_{cov} is an increasing function of $d_{h.c.}$ and SNR_1 . Since an

⁴From extensive simulations, we have checked that the observation window with $R > 20$ does not change the analysis significantly. Therefore, in this paper, we set $R = 20$. Note that the impact of the transmitters located further away will be diminished for larger values of α and smaller values of λ_1 and λ_2 . Therefore, we propose a choice of $R = 20$ when $\alpha \geq 4$, and λ_1 and λ_2 are no larger than the values adopted in our simulation settings. In other cases, the window radius R should be increased.

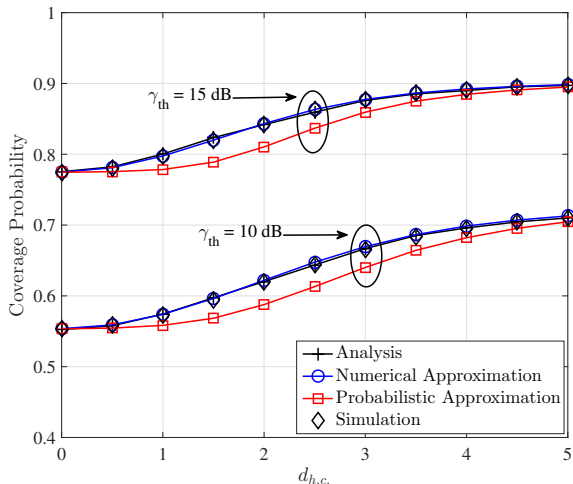


Fig. 4. Approximations of the coverage probability of single-tier networks as a function of $d_{h.c.}$.

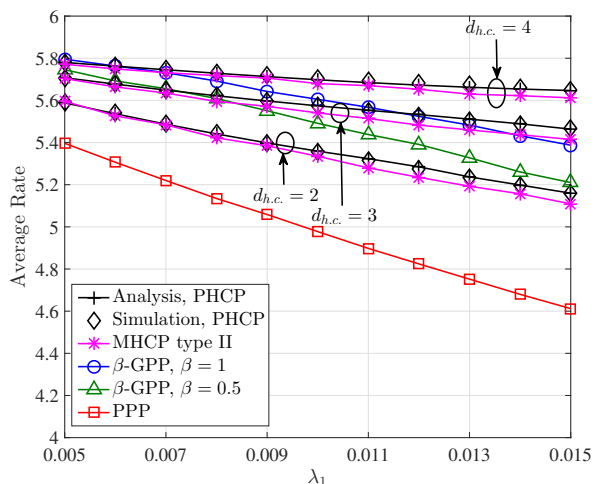


Fig. 5. Average rate of single-tier networks as a function of λ_1 .

increase in λ_1 results in additional interference, \mathcal{P}_{cov} decreases as λ_1 becomes bigger. Moreover, it is shown that \mathcal{P}_{cov} is more sensitive to $d_{h.c.}$ when the SNR_1 is large. Note that the impact of interference on the SINR in (12) becomes lower as $d_{h.c.}$ increases. Therefore, we can see that \mathcal{P}_{cov} is saturated when $d_{h.c.}$ is high, and the influence of λ_1 on \mathcal{P}_{cov} gets smaller as $d_{h.c.}$ becomes larger.

Fig. 4 reveals the tightness of the approximations of the coverage probability of the single-tier networks with $\text{SNR}_1 = 20$ dB and $\lambda_1 = 0.01$. First, we can see that our numerical approximation in (25) is very tight for all simulated configurations. Additionally, it is shown that the probabilistic approximation in (28), which is obtained by approximating the interference field as a PPP, exhibits small performance gaps compared to the simulated results. Moreover, we can observe that the probabilistic approximation becomes more tighter when $d_{h.c.}$ is small or large.

Fig. 5 establishes the average rate $\mathbb{E}[\log_2(1 + \gamma)]$ of the single-tier networks with $\text{SNR}_1 = 20$ dB. In this figure, we compare the performance of the networks with PHCPs with that of networks with β -GPPs, MHCPs of type II or a PPP. Note that a β -GPP with $\beta = 0$, a PHCP with $d_{h.c.} = 0$ and an MHCP with $d_{h.c.} = 0$ correspond to a PPP with the same intensity. Here, the analytical results for the networks with PHCPs are calculated by evaluating $\mathbb{E}[\log_2(1 + \gamma)] = \int_0^\infty \mathbb{P}(\gamma > 2^t - 1) dt$ where the integrand is computed by the result in Corollary 1. Also, the reduced Palm measure of β -GPPs is obtained by [44]. First, we see that the PPP yields the worst

performance as it cannot take a repulsive behavior into account. Also, since a larger β results in a stronger repulsion, it is shown that the average rate with the β -GPP increases with β . However, since the slopes corresponding to β -GPPs are higher than those corresponding to PHCPs, we infer that the PHCP is more efficient to alleviate the interference as λ_1 becomes larger. Moreover, when compared to the β -GPP, it is shown that the PHCP can model the case where there exists a strong repulsion since the β -GPP is only applicable to β such that $0 < \beta \leq 1$. In addition, we can see that two HCPs, the PHCP and the MHCP, exhibit almost the same trend. From the fact that the exact performance analysis of the networks with an MHCP is intractable, we can conclude that the PHCP is a more suitable model to analyze the wireless networks with a repulsion.

In Figs. 6 to 8, we present the coverage probability of two-tier networks where $\text{SNR}_1 = 20$ dB and $\lambda_1 = 0.01$. In Fig. 6, we illustrate the coverage probability when $\gamma_{th} = 15$ dB and $d_G = d_{h.c.}/2$. It is shown that the analytical result in (15) is very accurate for different values of $d_{h.c.}$, λ_2 and SNR_2 . We note that, when $d_{h.c.} = 0$, the two-tier networks with a PHCP and a guard zone become equivalent to the networks consisting of two independent PPPs with intensities λ_1 and λ_2 , respectively. Thus, from Fig. 6, we see that the network performance can be significantly enhanced by taking the PHCP and guard zone into account. As expected, the coverage probability \mathcal{P}_{cov} is a decreasing function of SNR_2 and λ_2 since a growth of SNR_2 (or λ_2) leads to an increase of interference. In addition, it is observed that the influence of λ_2 on \mathcal{P}_{cov} becomes smaller as $d_{h.c.}$ increases and SNR_2 decays.

In Fig. 7, we plot the average rate $\mathbb{E}[\log_2(1 + \gamma)]$ of the two-tier networks with $d_{h.c.} = 5$. The analytical results are obtained by evaluating $\mathbb{E}[\log_2(1 + \gamma)] = \int_0^\infty \mathbb{P}(\gamma > 2^t - 1) dt$ and using the result in Theorem 1. As expected, we see that the average rate is a decreasing function of λ_2 and SNR_2 . Since a larger d_G results in a reduced interference from the transmitters in the second-tier network, the average rate becomes higher as d_G gets bigger. In addition, it is observed that the impact of d_G is more pronounced when λ_2 is high as the inter-tier interference dominates the performance when λ_2 is large.

Fig. 8 reveals the exact and approximated coverage probabilities when $\text{SNR}_2 = 20$ dB, $\gamma_{th} = 10$ dB and $d_G = d_{h.c.}/2$. First, it is seen that our numerical approximation in (23) exhibits almost identical performance with the simulated result. Unlike the case in Fig 4, for two-tier networks, the performance gap between the simulated result and the probabilistic approximation is not

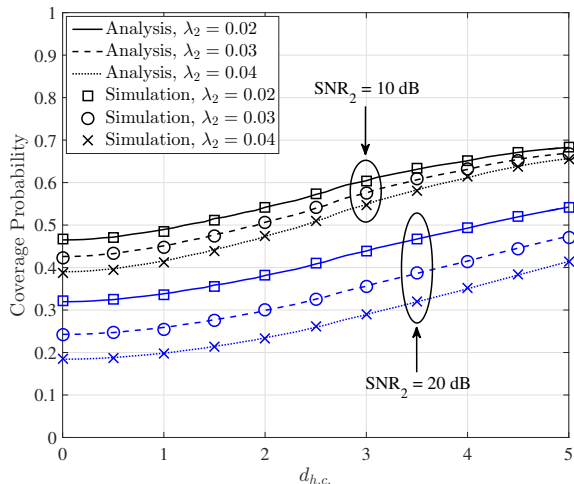


Fig. 6. Coverage probability of two-tier networks as a function of $d_{h.c.}$.

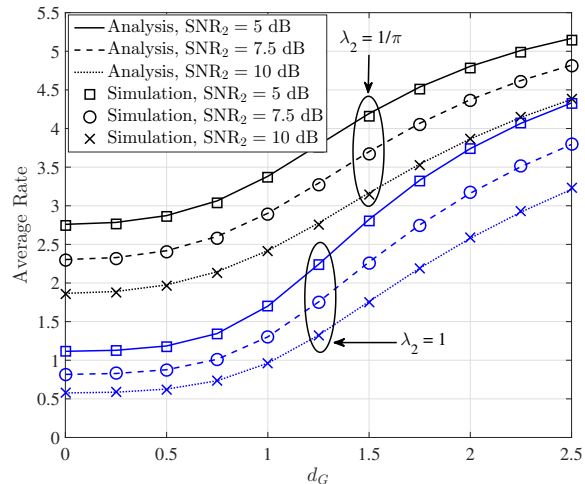


Fig. 7. Average rate of two-tier networks as a function of d_G .

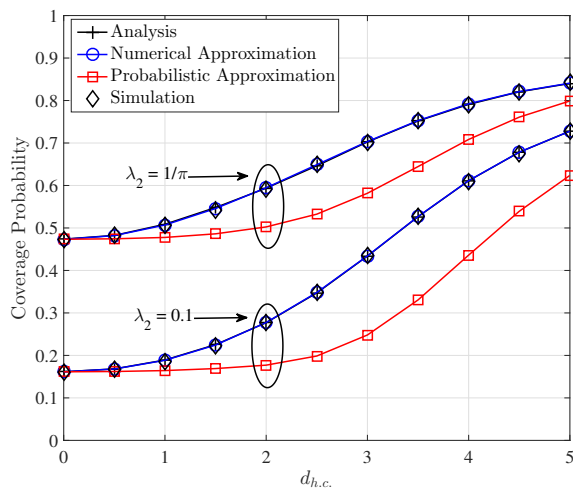


Fig. 8. Approximations of the coverage probability of two-tier networks as a function of $d_{h.c.}$.

small. This is due to the assumption in (29) that the interference from the second-tier network I_2 is independent from the one generated by the first-tier network I_1 . Indeed, the spatial distribution of the activated transmitters in the second-tier network Ψ_2^a is closely related to the locations of the transmitters in the first-tier network Ψ_1^0 . Lastly, we see that the probabilistic approximation gets tighter as λ_2 increases.

VI. CONCLUSION

In this paper, we have modeled two-tier heterogeneous networks using the Poisson hard-core process (PHCP) which takes the repulsion among the transmitters into account. We have investigated both single- and two-tier networks and considered a guard zone which alleviates the cross-tier interference. Under this setup, the distribution of the activated second-tier transmitters can be modeled as a Poisson hard-core hole process (PHCHP). We have derived explicit analytical expressions of the coverage probability for both single-/two-tier networks. In addition, we have introduced the method to compute the derived results by employing the Quasi-Monte Carlo (QMC) technique. Different approximations of the coverage probability which have low computational complexities have also been provided. In the simulation results, we have verified that our analysis accurately predicts the performance and confirmed that the coverage probability is an increasing function of the radius of the PHCP.

APPENDIX A

PROOF OF LEMMA 1

Let us denote by $\tilde{\lambda}(\lambda, d)$ the scaled intensity. Then, the equation characterizing $\tilde{\lambda}(\lambda, d)$ is

$$\mathbb{E}[\Psi_1^0(W)] = \tilde{\lambda}(\lambda, d)\pi R^2. \quad (33)$$

From (3) and (8),

$$c^{-1} = \sum_{n \geq 0} \frac{\lambda^n e^{-\pi R^2}}{n!} \int_{(W \setminus \mathcal{B}_0(d))^n} \prod_{\substack{j,k=1,\dots,n; \\ j \neq k}} \mathbb{1}_{\{\|\mathbf{x}_j - \mathbf{x}_k\| \geq d\}} d\mathbf{x}_1 \cdots d\mathbf{x}_n = \sum_{n \geq 0} \frac{\lambda^n e^{-\pi R^2}}{n!} \nu_n, \quad (34)$$

and we have

$$\begin{aligned} \mathbb{E}[\Psi_1^0(W)] &= c \sum_{n \geq 0} \frac{n e^{-\pi R^2}}{n!} \int_{(W \setminus \mathcal{B}_0(d_{h.c.}))^n} f_{\Psi_1^0}(\{\mathbf{x}_1, \dots, \mathbf{x}_n\}) d\mathbf{x}_1 \cdots d\mathbf{x}_n \\ &= c \sum_{n \geq 0} \frac{n \lambda^n e^{-\pi R^2}}{n!} \nu_n = c \lambda \sum_{n \geq 0} \frac{\lambda^n e^{-\pi R^2}}{n!} \nu_{n+1}. \end{aligned} \quad (35)$$

Hence, from (33)-(35), $\tilde{\lambda}(\lambda, d)$ is given by (9). ■

APPENDIX B
PROOF OF THEOREM 1

We recall that the coverage probability is computed by (14), and thus in this proof we focus on the computation of the Laplace transform \mathcal{L}_I . For any $s > 0$, from the fact that the laws of Ψ_1^0 and Ψ_2 are invariant with respect to rotations, we derive the Laplace transform $\mathcal{L}_I(s)$ as

$$\mathcal{L}_I(s) = \mathbb{E} \left[\exp \left(-s \left(\sum_{\mathbf{y} \in \Psi_1^0} P_1 h_{\mathbf{y}} \|\mathbf{y} - (r_1, 0)\|^{-\alpha} + \sum_{\mathbf{z} \in \Psi_2^a} P_2 h_{\mathbf{z}} \|\mathbf{z} - (r_1, 0)\|^{-\alpha} \right) \right) \right].$$

Therefore, we have

$$\begin{aligned} \mathcal{L}_I(s) &= \mathbb{E} \left[\prod_{\mathbf{y} \in \Psi_1^0} \mathbb{E} \left[\exp \left(-s P_1 h_{\mathbf{y}} \|\mathbf{y} - (r_1, 0)\|^{-\alpha} \right) \right] \right. \\ &\quad \times \left. \prod_{\mathbf{z} \in \Psi_2^a} \mathbb{E} \left[\exp \left(-s P_2 h_{\mathbf{z}} \|\mathbf{z} - (r_1, 0)\|^{-\alpha} \right) \mid \Psi_1^0, \Psi_2 \right] \right] \\ &= \mathbb{E} \left[\prod_{\mathbf{y} \in \Psi_1^0} \frac{1}{1 + s P_1 \|\mathbf{y} - (r_1, 0)\|^{-\alpha}} \prod_{\mathbf{z} \in \Psi_2^a} \frac{1}{1 + s P_2 \|\mathbf{z} - (r_1, 0)\|^{-\alpha}} \right] \\ &= \mathbb{E} \left[\exp \left(- \sum_{\mathbf{y} \in \Psi_1^0} \ln \left(1 + s P_1 \|\mathbf{y} - (r_1, 0)\|^{-\alpha} \right) \right) \right. \\ &\quad \times \left. \mathbb{E} \left[\exp \left(- \sum_{\mathbf{z} \in \Psi_2} \ln \left(1 + s P_2 \|\mathbf{z} - (r_1, 0)\|^{-\alpha} \right) \mathbb{1}_{\{\mathbf{z} \notin \Xi\}} \right) \mid \Psi_1^0 \right] \right]. \end{aligned}$$

Then, we compute the probability generation functional (PGFL) of the PPP [3] and deduce

$$\begin{aligned} \mathcal{L}_I(s) &= \mathbb{E} \left[\exp \left(- \sum_{\mathbf{y} \in \Psi_1^0} \ln \left(1 + s P_1 \|\mathbf{y} - (r_1, 0)\|^{-\alpha} \right) \right) \right. \\ &\quad \times \left. \exp \left(- \lambda_2 \int_W \frac{1}{1 + (s P_2)^{-1} \|\mathbf{z} - (r_1, 0)\|^{-\alpha}} \mathbb{1}_{\{\mathbf{z} \notin \Xi\}} d\mathbf{z} \right) \right] \\ &= \exp \left(- \lambda_2 \int_W \frac{1}{1 + (s P_2)^{-1} \|\mathbf{z} - (r_1, 0)\|^{-\alpha}} d\mathbf{z} \right) \\ &\quad \times \mathbb{E} \left[\exp \left(- \sum_{\mathbf{y} \in \Psi_1^0} \left(\ln \left(1 + s P_1 \|\mathbf{y} - (r_1, 0)\|^{-\alpha} \right) + \lambda_2 \int_W \frac{1}{1 + (s P_2)^{-1} \|\mathbf{z} - (r_1, 0)\|^{-\alpha}} \mathbb{1}_{\{\mathbf{z} \in \Xi\}} d\mathbf{z} \right) \right) \right] \\ &\stackrel{(a)}{=} \exp(-\lambda_2 \kappa) \mathbb{E} \left[\exp \left(- \sum_{\mathbf{y} \in \Psi_1^0} \left(\ln \left(1 + s P_1 \|\mathbf{y} - (r_1, 0)\|^{-\alpha} \right) + \lambda_2 \beta_{\mathbf{y}} \right) \right) \right], \quad (36) \end{aligned}$$

where $\kappa \triangleq \int_{\mathcal{B}_0(R) \setminus \mathcal{B}_0(d_G)} (1 + (s P_2)^{-1} \|\mathbf{y} - (r_1, 0)\|^{-\alpha})^{-1} d\mathbf{y}$ and $\beta_{\mathbf{y}} \triangleq \int_{\mathcal{B}_{\mathbf{y}}(d_G) \cap \mathcal{B}_0(R)} (1 + (s P_2)^{-1} \|\mathbf{z} - (r_1, 0)\|^{-\alpha})^{-1} d\mathbf{z}$. Here, (a) follows from the fact that the points in Ψ_1^0 cannot be closer than $d_{h.c.}$

from one another, which implies that

$$\mathbb{1}_{\{\mathbf{z} \in \Xi\}} = \mathbb{1}_{\{\mathbf{z} \in \mathcal{B}_0(d_G) \cup \bigcup_{\mathbf{y} \in \Psi_1^0} \mathcal{B}_{\mathbf{y}}(d_G)\}} = \mathbb{1}_{\{\mathbf{z} \in \mathcal{B}_0(d_G)\}} + \sum_{\mathbf{y} \in \Psi_1^0} \mathbb{1}_{\{\mathbf{z} \in \mathcal{B}_{\mathbf{y}}(d_G)\}},$$

since $d_G \leq d_{\text{h.c.}}/2$.

By Proposition 3 in Appendix D, we have

$$\begin{aligned} \kappa = 2\pi \int_{\max(d_G - r_1, 0)}^{R - r_1} \frac{r}{1 + (sP_2)^{-1}r^\alpha} dr + 2 \int_{R - r_1}^{r_1 + R} \frac{\arccos\left(\frac{r_1^2 + r^2 - R^2}{2r_1r}\right)}{1 + (sP_2)^{-1}r^\alpha} r dr \\ - 2 \int_{|d_G - r_1|}^{r_1 + d_G} \frac{\arccos\left(\frac{r_1^2 + r^2 - d_G^2}{2r_1r}\right)}{1 + (sP_2)^{-1}r^\alpha} r dr, \end{aligned} \quad (37)$$

and

$$\beta_{\mathbf{y}} = \int_0^{R+r_1} \frac{r}{1 + (sP_2)^{-1}r^\alpha} \theta_{\mathbf{y}}(r) dr. \quad (38)$$

Substituting (37) and (38) into (36), and applying (1), the Laplace transform in (36) is equal to

$$\begin{aligned} \mathcal{L}_I(s) &= \exp(-\lambda_2 \kappa) \mathbb{E} \left[\exp \left(- \sum_{\mathbf{y} \in \Psi_1^0} \left(\ln \left(1 + sP_1 \|\mathbf{y} - (r_1, 0)\| \right)^{-\alpha} \right) + \lambda_2 \int_0^{R+r_1} \frac{r}{1 + (sP_2)^{-1}r^\alpha} \theta_{\mathbf{y}}(r) dr \right) \right] \\ &= c \exp(-\lambda_2 \kappa) \sum_{n \geq 0} \frac{\lambda_1^n}{n!} \int_{(W \setminus \mathcal{B}_0(d_{\text{h.c.}}))^n} \prod_{i=1}^n \frac{1}{1 + sP_1 \|\mathbf{x}_i - (r_1, 0)\|^{-\alpha}} \\ &\quad \times \prod_{\substack{j,k=1,\dots,n; \\ j \neq k}} \mathbb{1}_{\{\|\mathbf{x}_j - \mathbf{x}_k\| \geq d_{\text{h.c.}}\}} \exp \left(\lambda_2 \sum_{i=1}^n \int_0^{R+r_1} \frac{r}{1 + (sP_2)^{-1}r^\alpha} \theta_{\mathbf{x}_i}(r) dr \right) d\mathbf{x}_1 \cdots d\mathbf{x}_n. \end{aligned} \quad (39)$$

Finally, by plugging (39) into (14), we obtain (15). \blacksquare

APPENDIX C

PROOF OF PROPOSITION 2

Let us denote the rotation of angle u by R_u . Since the law of Φ is invariant with respect to rotations, we have

$$\begin{aligned} f(\lambda, s, \tau) &= \frac{1}{2\pi} \int_0^{2\pi} \mathbb{E} \left[\exp \left(-s \sum_{\mathbf{y} \in \Phi} h_{\mathbf{y}} \|\mathbf{y} - R_u(r_1, 0)\|^{-\alpha} \mathbb{1}_{\{\|\mathbf{y} - R_u(r_1, 0)\| \geq \tau\}} \right) \right] du \\ &= \mathbb{E} \left[\exp \left(-s \sum_{\mathbf{y} \in \Phi} h_{\mathbf{y}} \|\mathbf{y} - (r_1, 0)\|^{-\alpha} \mathbb{1}_{\{\|\mathbf{y} - (r_1, 0)\| \geq \tau\}} \right) \right]. \end{aligned}$$

Then,

$$\begin{aligned}
f(\lambda, s, \tau) &= \mathbb{E} \left[\prod_{\mathbf{y} \in \Phi: \|\mathbf{y} - (r_1, 0)\| \geq \tau} \mathbb{E} [\exp(-sh_{\mathbf{y}} \|\mathbf{y} - (r_1, 0)\|^{-\alpha}) \mid \Phi] \right] \\
&\stackrel{(b)}{=} \mathbb{E} \left[\prod_{\mathbf{y} \in \Phi: \|\mathbf{y} - (r_1, 0)\| \geq \tau} \frac{1}{1 + s \|\mathbf{y} - (r_1, 0)\|^{-\alpha}} \right] \\
&= \exp \left(-\lambda \int_W \frac{1}{1 + s^{-1} \|\mathbf{z} - (r_1, 0)\|^\alpha} \mathbb{1}_{\{\|\mathbf{z} - (r_1, 0)\| \geq \tau\}} d\mathbf{z} \right) \\
&= \exp \left(-\lambda \int_{\mathcal{B}_{(-r_1, 0)}(R)} \frac{1}{1 + s^{-1} \|\mathbf{z}\|^\alpha} \mathbb{1}_{\{\|\mathbf{z}\| \geq \tau\}} d\mathbf{z} \right) \\
&= \exp \left(-\lambda \int_{\mathcal{B}_{(-r_1, 0)}(R)} \frac{1}{1 + s^{-1} \|\mathbf{z}\|^\alpha} d\mathbf{z} + \lambda \int_{\mathcal{B}_0(\tau)} \frac{1}{1 + s^{-1} \|\mathbf{z}\|^\alpha} d\mathbf{z} \right) \\
&\stackrel{(c)}{=} \exp \left(-2\pi\lambda \int_\tau^{R-r_1} \frac{r}{1 + s^{-1} r^\alpha} dr - 2\lambda \int_{R-r_1}^{r_1+R} \frac{\arccos\left(\frac{r_1^2 + r^2 - R^2}{2r_1 r}\right)}{1 + s^{-1} r^\alpha} r dr \right),
\end{aligned}$$

where (b) follows from the independence of $\{h_{\mathbf{y}}\}$ and Φ , and the fact that the moment generating function of $h_{\mathbf{y}}$ is equal to $\mathbb{E}[\exp(th_{\mathbf{y}})] = (1 - t)^{-1}$. Lastly, to obtain (c), we have applied Proposition 3 in Appendix D. \blacksquare

APPENDIX D

A GEOMETRIC RESULT

In this appendix, we state and prove a technical result.

Proposition 3. *Let $\mathbf{y} \in \mathbb{R}^2$ and $d_G > 0$ be the center of a disk and its radius, respectively. Let R be such that $\|\mathbf{y}\| \leq R$ let $r_1 \geq 0$ be fixed, and let $f : \mathbb{R} \rightarrow [0, \infty)$ be a non-negative measurable function. Then, we have*

$$\int_{\mathcal{B}_{\mathbf{y}}(d_G) \cap \mathcal{B}_0(R)} f(\|\mathbf{x} - (r_1, 0)\|) d\mathbf{x} = \int_0^{R+r_1} r f(r) \theta_{\mathbf{y}}(r) dr. \quad (40)$$

Here, if $r \leq R - r_1$,

$$\theta_{\mathbf{y}}(r) = \begin{cases} 2\pi, & \text{if } 0 \leq r \leq \max(0, d_G - \|\mathbf{y} - (r_1, 0)\|), \\ 2 \arccos\left(\frac{\|\mathbf{y} - (r_1, 0)\|^2 + r^2 - d_G^2}{2\|\mathbf{y} - (r_1, 0)\| r}\right), & \text{if } |d_G - \|\mathbf{y} - (r_1, 0)\|| \leq r \leq d_G + \|\mathbf{y} - (r_1, 0)\|, \\ 0, & \text{otherwise,} \end{cases}$$

and otherwise, $\theta_{\mathbf{y}}(r)$ is equal to

$$\max\left(0, \arccos\left(\frac{\|\mathbf{y} - (r_1, 0)\|^2 + r^2 - d_G^2}{2\|\mathbf{y} - (r_1, 0)\|r}\right) + \min\left(\arccos\left(\frac{\|\mathbf{y} - (r_1, 0)\|^2 + r^2 - d_G^2}{2\|\mathbf{y} - (r_1, 0)\|r}\right), \arccos\left(\frac{r_1^2 + r^2 - R^2}{2r_1r}\right) - \arccos\left(\frac{\|\mathbf{y} - (r_1, 0)\|^2 + r_1^2 - \|\mathbf{y}\|^2}{2\|\mathbf{y} - (r_1, 0)\|r_1}\right)\right)\right),$$

if $r \in [\|\mathbf{y} - (r_1, 0)\| - d_G, \|\mathbf{y} - (r_1, 0)\| + d_G]$, and $\theta_{\mathbf{y}}(r) = 0$ otherwise. In particular, for any $d \geq 0$, we obtain

$$\int_{\mathcal{B}_{\mathbf{y}}(d)} f(\|\mathbf{x}\|) d\mathbf{x} = 2\pi \int_0^{\max(d-\|\mathbf{y}\|, 0)} r f(r) dr + 2 \int_{|d-\|\mathbf{y}\||}^{\|\mathbf{y}\|+d} r f(r) \arccos\left(\frac{\|\mathbf{y}\|^2 + r^2 - d^2}{2\|\mathbf{y}\|r}\right) dr. \quad (41)$$

Proof. Note that

$$\begin{aligned} \int_{\mathcal{B}_{\mathbf{y}}(d_G) \cap \mathcal{B}_0(R)} f(\|\mathbf{x} - (r_1, 0)\|) d\mathbf{x} &= \int_{\mathcal{B}_{\mathbf{y}-(r_1, 0)}(d_G) \cap \mathcal{B}_{(-r_1, 0)}(R)} f(\|\mathbf{x}\|) d\mathbf{x} \\ &= \int_0^\infty \int_0^{2\pi} f(r) \mathbb{1}_{\{(r \cos(\theta), r \sin(\theta)) \in \mathcal{B}_{\mathbf{y}-(r_1, 0)}(d_G) \cap \mathcal{B}_{(-r_1, 0)}(R)\}} r d\theta dr = \int_0^\infty r f(r) \theta_{\mathbf{y}}(r) dr, \end{aligned}$$

where $\theta_{\mathbf{y}}(r) \in [0, 2\pi]$ is the angle covered by the portion of the circle centered at the origin and of radius r that is in $\mathcal{B}_{\mathbf{y}-(r_1, 0)}(d_G) \cap \mathcal{B}_{(-r_1, 0)}(R)$.

Assume first that $\|\mathbf{y} - (r_1, 0)\| \leq R - d_G - r_1$ (which implies $\mathcal{B}_{\mathbf{y}-(r_1, 0)}(d_G) \subset \mathcal{B}_{(-r_1, 0)}(R)$) or $r \leq R - r_1$ (which implies $\mathcal{B}_0(r) \subset \mathcal{B}_{(-r_1, 0)}(R)$), and let us distinguish two cases.

- 1) First, assume that $\|\mathbf{y} - (r_1, 0)\| \geq d_G$. If $r < \|\mathbf{y} - (r_1, 0)\| - d_G$ or $r > \|\mathbf{y} - (r_1, 0)\| + d_G$, the circle centered at the origin of radius r does not intersect $\mathcal{B}_{\mathbf{y}-(r_1, 0)}(d_G)$, and thus $\theta_{\mathbf{y}}(r) = 0$. Else, defining $\theta_1(r)$ and $\theta_2(r)$ as in Fig. 9-(a), by the cosine law in the triangle ABC , we have $d_G^2 = \|\mathbf{y} - (r_1, 0)\|^2 + r^2 - 2\|\mathbf{y} - (r_1, 0)\|r \cos(\theta_1(r))$. Also, similarly by the cosine law in ABD , we have $d_G^2 = \|\mathbf{y} - (r_1, 0)\|^2 + r^2 - 2\|\mathbf{y} - (r_1, 0)\|r \cos(\theta_2(r))$. Hence, we conclude that in this case

$$\theta_{\mathbf{y}}(r) = 2 \arccos\left(\frac{\|\mathbf{y} - (r_1, 0)\|^2 + r^2 - d_G^2}{2\|\mathbf{y} - (r_1, 0)\|r}\right), \quad (42)$$

for $r \in [\|\mathbf{y} - (r_1, 0)\| - d_G, \|\mathbf{y} - (r_1, 0)\| + d_G]$.

- 2) Second, assume that $\|\mathbf{y} - (r_1, 0)\| < d_G$. Then, when $r \leq d_G - \|\mathbf{y} - (r_1, 0)\|$, $\mathcal{B}_0(r) \subset \mathcal{B}_{\mathbf{y}-(r_1, 0)}(d_G)$, and thus $\theta_{\mathbf{y}}(r) = 2\pi$. Else, when $d_G - \|\mathbf{y} - (r_1, 0)\| < r \leq d_G - \|\mathbf{y} + (r_1, 0)\|$, by the same arguments as in the first part, (42) holds.

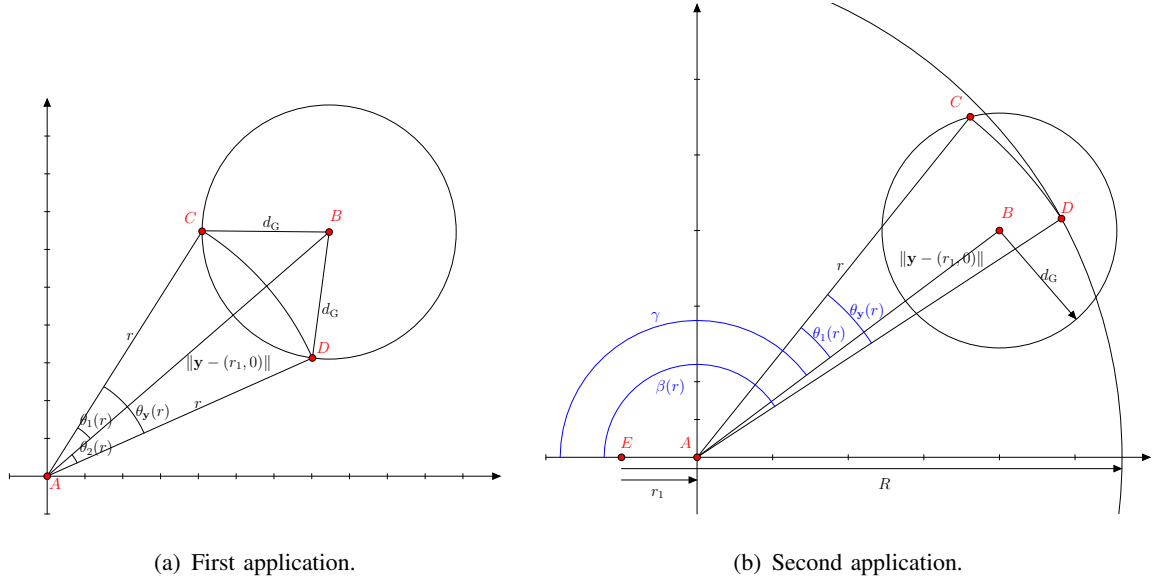


Fig. 9. Cosine law.

By the above two steps, we obtain

$$\theta_{\mathbf{y}}(r) = \begin{cases} 2\pi & \text{if } 0 \leq r \leq \max(0, d_G - \|\mathbf{y} - (r_1, 0)\|), \\ 2 \arccos\left(\frac{\|\mathbf{y} - (r_1, 0)\|^2 + r^2 - d_G^2}{2\|\mathbf{y} - (r_1, 0)\|r}\right) & \text{if } |d_G - \|\mathbf{y} - (r_1, 0)\|| \leq r \leq d_G + \|\mathbf{y} - (r_1, 0)\|, \\ 0 & \text{otherwise.} \end{cases} \quad (43)$$

Assume now that $\|\mathbf{y} - (r_1, 0)\| > R - d_G - r_1$ and $r > R - r_1$. If $r > \min(R + r_1, \|\mathbf{y} - (r_1, 0)\| + d_G)$ or $r \leq \|\mathbf{y} - (r_1, 0)\| - d_G$, the circle centered at the origin of radius r does not intersect either $\mathcal{B}_{\mathbf{y} - (r_1, 0)}(d_G)$ or $\mathcal{B}_{(-r_1, 0)}(R)$, and thus $\theta_{\mathbf{y}}(r) = 0$. Else, we consider the setting and notation of Fig. 9-(b). In this case, we have

$$\theta_{\mathbf{y}}(r) = \begin{cases} 2\theta_1(r) & \text{if } \beta(r) - \gamma \geq \theta_1(r), \\ \theta_1(r) + \beta(r) - \gamma & \text{if } -\theta_1(r) \leq \beta(r) - \gamma < \theta_1(r), \\ 0 & \text{otherwise,} \end{cases}$$

and it is readily checked that this can be rewritten as $\theta_{\mathbf{y}}(r) = \max(0, \theta_1(r) + \min(\theta_1(r), \beta(r) - \gamma))$. The angle $\theta_1(r)$ has already been seen to be equal to $\arccos((\|\mathbf{y} - (r_1, 0)\|^2 + r^2 - d_G^2)/2\|\mathbf{y} - (r_1, 0)\|r)$. Additionally, by an application of the cosine law in the triangles ADE and ABE

respectively, we obtain

$$\beta(r) = \arccos\left(\frac{r^2 + r_1^2 - R^2}{2r_1r}\right) \quad \text{and} \quad \gamma = \arccos\left(\frac{\|\mathbf{y} - (r_1, 0)\|^2 + r_1^2 - \|\mathbf{y}\|^2}{2\|\mathbf{y} - (r_1, 0)\|r_1}\right).$$

Let us summarize the obtained results. When $r \leq R - r_1$, $\theta_{\mathbf{y}}(r)$ is given by (43). When $r > R - r_1$ and $\|\mathbf{y} - (r_1, 0)\| \leq R - d_G - r_1$, we necessarily have $r > \|\mathbf{y} - (r_1, 0)\| + d_G$ and therefore $\theta_{\mathbf{y}}(r) = 0$. When $r > R - r_1$ and $\|\mathbf{y} - (r_1, 0)\| > R - d_G - r_1$, we have

$$\theta_{\mathbf{y}}(r) = \max(0, \theta_1(r) + \min(\theta_1(r), \beta(r) - \gamma)) \mathbb{1}_{\{r \in [\|\mathbf{y} - (r_1, 0)\| - d_G, \min(R + r_1, \|\mathbf{y} - (r_1, 0)\| + d_G)\]}.$$

This concludes the proof of the result in (40). In order to obtain (41), it suffices to choose $r_1 = 0$ and let R go to infinity in the result (40). \square

REFERENCES

- [1] H.-B. Kong, I. Flint, P. Wang, D. Niyato, and N. Privault, "Modeling and analysis of wireless networks using Poisson hard-core process," presented at *IEEE Int. Conf. on Commun. (ICC)*, Paris, France, May 2017.
- [2] J. G. Andrews, S. Buzzi, W. Choi, S. V. Hanly, A. Lozano, A. C. K. Soong, and J. C. Zhang, "What will 5G be?," *IEEE J. Sel. Areas Commun.*, vol. 32, pp. 1065–1082, Jun. 2014.
- [3] M. Haenggi, *Stochastic geometry for wireless networks*. Cambridge, U.K.: Cambridge Univ. Press, 2012.
- [4] A. Wyner, "Shannon-theoretic approach to a Gaussian cellular multiple-access channel," *IEEE Trans. Inf. Theory*, vol. 40, pp. 1713–1727, Nov. 1994.
- [5] A. M. Hunter, J. G. Andrews, and S. Weber, "Transmission capacity of ad hoc networks with spatial diversity," *IEEE Trans. Wireless Commun.*, vol. 12, pp. 5058–5071, Dec. 2008.
- [6] S. Weber, J. G. Andrews, and N. Jindal, "An overview of the transmission capacity of wireless networks," *IEEE Trans. Commun.*, vol. 58, pp. 3593–3604, Dec. 2010.
- [7] J. G. Andrews, F. Baccelli, and R. K. Ganti, "A tractable approach to coverage and rate in cellular networks," *IEEE Trans. Commun.*, vol. 59, pp. 3122–3134, Nov. 2011.
- [8] T. D. Novlan, H. S. Dhillon, and J. G. Andrews, "Analytical modeling of uplink cellular networks," *IEEE Trans. Wireless Commun.*, vol. 12, pp. 2669–2679, Jun. 2013.
- [9] H. S. Dhillon, R. K. Ganti, F. Baccelli, and J. G. Andrews, "Modeling and analysis of K -tier downlink heterogeneous cellular networks," *IEEE J. Sel. Areas Commun.*, vol. 30, pp. 550–560, Apr. 2012.
- [10] H.-S. Jo, Y. J. Sang, P. Xia, and J. G. Andrews, "Heterogeneous cellular networks with flexible cell association: A comprehensive downlink SINR analysis," *IEEE Trans. Wireless Commun.*, vol. 11, pp. 3484–3495, Oct. 2012.
- [11] C. Li, J. Zhang, J. G. Andrews, and K. B. Letaief, "Success probability and area spectral efficiency in multiuser MIMO HetNets," *IEEE Trans. Commun.*, vol. 64, pp. 1544–1556, Apr. 2016.
- [12] H. ElSawy and E. Hossain, "On stochastic geometry modeling of cellular uplink transmission with truncated channel inversion power control," *IEEE Trans. Wireless Commun.*, vol. 13, pp. 4454–4469, Aug. 2014.
- [13] A. M. Ibrahim, T. A. ElBatt, and A. El-Keyi, "Coverage probability analysis for wireless networks using repulsive point processes," in *Proc. Int. Symp. Personal, Indoor and Mobile radio communications, London, United Kingdom*, pp. 1002–1007, Sep. 2013.

- [14] D. B. Taylor, H. S. Dhillon, T. D. Novlan, and J. G. Andrews, "Pairwise interaction processes for modeling cellular network Topology," in *Proc. IEEE Global Commun. Conf. (Globecom)*, pp. 4524–4529, Dec. 2012.
- [15] A. Guo and M. Haenggi, "Spatial stochastic models and metrics for the structure of base stations in cellular networks," *IEEE Trans. Wireless Commun.*, vol. 12, pp. 5800–5812, Nov. 2013.
- [16] Q. Ying, Z. Zhao, Y. Zhou, R. Li, X. Zhou, and H. Zhang, "Characterizing spatial patterns of base stations in cellular networks," in *Proc. IEEE/CIC International Conference on communications in China (ICCC)*, Oct. 2014, pp. 490–495.
- [17] M. Afshang and H. S. Dhillon, "Poisson Cluster Process Based Analysis of HetNets with Correlated User and Base Station Locations," 2017. Available: arXiv:1612.07285v2.
- [18] Y. Li, F. Baccelli, H. S. Dhillon, and J. G. Andrews, "Statistical modeling and probabilistic analysis of cellular networks with determinantal point processes," *IEEE Trans. Commun.*, vol. 63, pp. 3405–3422, Sep. 2015.
- [19] N. Miyoshi and T. Shirai, "A cellular network model with Ginibre configured base stations," *Adv. in Appl. Probab.*, vol. 46, pp. 832–845, 2004.
- [20] N. Deng, W. Zhou, and M. Haenggi, "The Ginibre point process as a model for wireless networks with repulsion," *IEEE Trans. Wireless Commun.*, vol. 14, pp. 107–121, Jan. 2015.
- [21] H. B. Kong, I. Flint, P. Wang, D. Niyato, and N. Privault, "Exact performance analysis of ambient RF energy harvesting wireless sensor networks with Ginibre point process," *IEEE J. Sel. Areas Commun.*, vol. 34, pp. 3769–3784, Dec. 2016.
- [22] B. Matérn, *Spatial Variation*. Springer lecture notes in statistics, 1986.
- [23] F. Lagum, S. S. Szyszkowicz, and H. Yanikomeroglu, "CoV-based metrics for quantifying the regularity of hard-core point processes for modeling base Station Locations," *IEEE Wireless Commun. Lett.*, vol. 5, pp. 276–279, Jun. 2016.
- [24] M. Haenggi, "Mean interference in hard-core wireless networks," *IEEE Commun. Lett.*, vol. 15, pp. 792–694, Aug. 2011.
- [25] B. Cho, K. Koufos, and R. Jäntti, "Bounding the mean interference in Matérn Type II hard-core wireless networks," *IEEE Commun. Lett.*, vol. 2, pp. 563–566, Oct. 2013.
- [26] A. Al-Hourani, R. J. Evans, and S. Kandeepan, "Nearest neighbour distance distribution in hard-core point processes," *IEEE Commun. Lett.*, vol. 20, pp. 1872–1875, Sep. 2016.
- [27] H. Q. Nguyen, F. Baccelli, and D. Kofman, "A stochastic geometry analysis of dense IEEE 802.11 networks," in *Proc. IEEE INFOCOM 2007*, pp. 1199–1207, Oct. 2007.
- [28] H. He, J. Xue, T. Ratnarajah, F. A. Khan, and C. B. Papadias, "Modeling and analysis of cloud radio access networks using Matérn hard-core point processes," *IEEE Trans. Wireless Commun.*, vol. 6, pp. 4074–4087, Jun. 2016.
- [29] H. ElSawy and E. Hossain, "Two-tier HetNets with cognitive femtocells: Downlink performance modeling and analysis in a multichannel environment," *IEEE Trans. Mobile Comput.*, vol. 13, pp. 649–663, Mar. 2014.
- [30] A. Hasan and J. G. Andrews, "The guard zone in wireless ad hoc networks," *IEEE Trans. Wireless Commun.*, vol. 6, pp. 897–906, Mar. 2007.
- [31] C.-H. Lee and M. Haenggi, "Interference and outage in Poisson cognitive networks," *IEEE Trans. Wireless Commun.*, vol. 11, pp. 1392–1401, Apr. 2012.
- [32] U. Tefek and T. J. Lim, "Interference management through exclusion zones in two-tier cognitive networks," *IEEE Trans. Wireless Commun.*, vol. 15, pp. 2292–2302, Mar. 2016.
- [33] N. Deng, W. Zhou, and M. Haenggi, "Heterogeneous cellular network models with dependence," *IEEE J. Sel. Areas Commun.*, vol. 33, pp. 2167–2181, Oct. 2015.
- [34] H. Sun, M. Wildemeersch, M. Sheng, and T. Q. S. Quek, "D2D enhanced heterogeneous cellular networks with dynamic TDD," *IEEE Trans. Wireless Commun.*, vol. 8, pp. 4204–4218, Aug. 2015.
- [35] Z. Yazdanshenasan, H. S. Dhillon, M. Afshang, and P. H. J. Chong, "Poisson hole process: Theory and applications to wireless networks," *IEEE Trans. Wireless Commun.*, vol. 15, pp. 7531–7546, Nov. 2016.

- [36] O. Kallenberg, *Random measures*. Fourth Edition, Berlin, Germany: Akademie-Verlag, 1986.
- [37] D. J. Daley and D. Vere-Jones, *An introduction to the theory of point processes: Volume II: general theory and structure*. Second Edition, New York: Springer, 2008.
- [38] K. K. Berthelsen and J. Møller, “A primer on perfect simulation for spatial point processes,” *Bulletin of the Brazilian Mathematical Society*, vol. 33, pp. 351–367, Nov. 2002.
- [39] N. Devroye, M. Vu, and V. Tarokh, “Cognitive radio networks: Highlights of information theoretic limits, models and design,” *IEEE Signal process. Mag.*, vol. 25, pp. 12–23, Nov. 2008.
- [40] F. Y. Kuo and I. H. Sloan, “Lifting the curse of dimensionality,” *Notices AMS*, vol. 52, pp. 1320–1328, 2005.
- [41] B. Blaszczyszyn and H. P. Keeler, “Studying the SINR process of the typical user in Poisson networks by using its factorial moment measures,” 2014. Available: <https://arxiv.org/abs/1401.4005>.
- [42] M. Haenggi and R. Ganti, “Interference in large wireless networks,” *Foundations and Trends in networking*, vol. 3, pp. 127–248, 2008.
- [43] R. E. Caflisch, *Monte Carlo and Quasi-Monte Carlo methods*. Cambridge, U.K.: Cambridge Univ. Press, 1998.
- [44] T. Shirai and Y. Takahashi, “Random point fields associated with certain Fredholm determinants I: Fermion, Poisson and boson point processes,” *J. Functional Anal.*, vol. 205, pp. 414–463, Apr. 2003.